remote sensing

MDPI

Article

An Innovative Tool for Monitoring Mangrove Forest Dynamics in Cuba Using Remote Sensing and WebGIS Technologies: SIGMEM

Alexey Valero-Jorge [1], Raúl González-Lozano [2], Roberto González-De Zayas [3,4], Felipe Matos-Pupo [5], Rogert Sorí [6] and Milica Stojanovic [6,*]

[1] Department of Agricultural Systems, Forestry and Environment (Unit Associated to EEAD-CSIC Soils and Irrigation), Center for Agri-Food Research and Technology of Aragon (CITA), 50059 Zaragoza, Spain; avalero@cita-aragon.es
[2] Independent Researcher, Santa Clara 50100, Cuba; arodriguez@aiscosolutions.com
[3] Department of Hydraulic Engineering, Faculty of Technical Sciences, Universidad de Ciego de Ávila, Ciego de Ávila 65100, Cuba; robertogz@unica.cu
[4] Centre for Geomatic, Environmental and Marine Estudies (GEOMAR), Ciudad de México 11560, Mexico
[5] Provincial Meteorological Centre of Ciego de Ávila, Institute of Meteorology, Avenida de los Deportes S/N, Ciego de Ávila 65100, Cuba; felipe.matos@cav.insmet.cu
[6] Centro de Investigación Mariña, Environmental Physics Laboratory (EPhysLab), Universidade de Vigo, Campus As Lagoas s/n, 32004 Ourense, Spain; rogert.sori@uvigo.es
* Correspondence: mstojanovic@uvigo.es

Abstract: The main objective of this work was to develop a viewer with web output, through which the changes experienced by the mangroves of the Gran Humedal del Norte de Ciego de Avila (GHNCA) can be evaluated from remote sensors, contributing to the understanding of the spatiotemporal variability of their vegetative dynamics. The achievement of this objective is supported by the use of open-source technologies such as MapStore, GeoServer and Django, as well as Google Earth Engine, which combine to offer a robust and technologically independent solution to the problem. In this context, it was decided to adopt an action model aimed at automating the workflow steps related to data preprocessing, downloading, and publishing. A visualizer with web output (Geospatial System for Monitoring Mangrove Ecosystems or SIGMEM) is developed for the first time, evaluating changes in an area of central Cuba from different vegetation indices. The evaluation of the machine learning classifiers Random Forest and Naive Bayes for the automated mapping of mangroves highlighted the ability of Random Forest to discriminate between areas occupied by mangroves and other coverages with an Overall Accuracy (OA) of 94.11%, surpassing the 89.85% of Naive Bayes. The estimated net change based on the year 2020 of the areas determined during the classification process showed a decrease of 5138.17 ha in the year 2023 and 2831.76 ha in the year 2022. This tool will be fundamental for researchers, decision makers, and students, contributing to new research proposals and sustainable management of mangroves in Cuba and the Caribbean.

Keywords: mangrove; Sentinel-2; webvisor; machine learning

Citation: Valero-Jorge, A.; González-Lozano, R.; González-De Zayas, R.; Matos-Pupo, F.; Sorí, R.; Stojanovic, M. An Innovative Tool for Monitoring Mangrove Forest Dynamics in Cuba Using Remote Sensing and WebGIS Technologies: SIGMEM. *Remote Sens.* **2024**, *16*, 3802. https://doi.org/10.3390/rs16203802

Academic Editor: Prasad S. Thenkabail

Received: 9 September 2024
Revised: 5 October 2024
Accepted: 10 October 2024
Published: 12 October 2024

1. Introduction

Ecosystems and their environmental services are increasingly vulnerable to significant transformations due to changes in the global climate. For example, shifts in temperature and precipitation regimes are expected to trigger environmental modifications, which will consequently affect the behavior of the organisms that in habitat these ecosystems. Thus, it is essential to plan and implement actions focused on protecting the valuable resources contained in these ecosystems. In comparison to larger land areas, the impacts and risks driven by climate change are often greater for small islands. This is primarily because they are surrounded by ocean, have relatively small land masses, and are frequently remote from more densely populated regions, which limits their global connectivity [1]. In the

Caribbean region, Cuba is an archipelago with the largest island of the same name in the region and it stands out for its extraordinary species richness and considerable level of endemism, ranking first in the West Indies for endemism of higher plants [2]. That is why Cuba has established a robust System of Protected Areas (PAs) that interacts both nationally and internationally. Among the Cuban PAs, wetlands stand out, with the Gran Humedal del Norte de Ciego de Ávila (GHNCA) among the most important. Due to its exceptional natural values, it was designated as the Ramsar Site No. 1235 on November 18, 2002, in agreement with Article 2.1 of the Convention on Wetlands [2].

Within the GHNCA, there are six PAs: Cayo Coco Central West Ecological Reserve, Monte El Coy Managed Floristic Reserve, Loma de Cunagua, El Venero, Laguna La Redonda, and Laguna de la Leche. The last four of these protected areas belong to the Fauna Refuge category due to migratory birds, endemic species, and endangered species protection. From a socioeconomic perspective, the richness of its marine platform and its landscape values makes this wetland home of one of the most important tourist centers in the country, Jardines del Rey. Additionally, it is also an important supplier of fishing resources.

One of the most relevant ecosystems within the GHNCA is the mangrove forest. It stands out for its extensive area, wide spatial distribution, and great variety of species it shelters. Mangroves also play an important role in facing disasters, acting as one of the four natural barriers that help to mitigate the impacts of waves generated by hurricanes that pass through the north. However, at the same time, hurricanes also negatively impact the health of mangroves. These considerations confirm the importance of mangroves and the need for their protection and conservation. [3].

In 2017, hurricane Irma caused large floods in several islands of the Caribbean, with significant differences between flooded areas in urbanized and non-urbanized sites. On Saint Martin Island, for example, the recovery of damaged mangroves was slower in healthy mangrove forests than that of those affected by anthropic development [4]. In Cuba, strong winds and coastal flooding generated by this system caused severe damage to coastal settlements. However, the town of Punta Alegre located in the northwest of Ciego de Avila province was protected by mangrove forests of the GHNCA, located to the north of the town [5].

The first spatial analyses of mangrove ecosystems began in the second half of the 20th century; however, despite their importance, it is a topic that is little studied to date. Godoy [6] studied the distribution and composition of a mangrove forest on the Pacific coast of Guatemala, and Jiménez [7] briefly described the mangrove communities on the coast of El Salvador. The study of mangroves in Cuba has been more focused on the use of data taken in fieldwork, and the application of remote sensing in the analysis of the spatiotemporal distribution of mangrove forests is recognized, given the potential and benefits of the technique in this type of research [8,9].

Currently, the most widespread method for studying and monitoring mangrove forests is through the application of remote sensing techniques (e.g., [10–12]), particularly when considering the high costs of resources involved in traditional field surveys [13] given the inaccessible nature, dynamics, and extent of these ecosystems [14,15]. Given the vast size of Cuba and the extensive area occupied by mangroves (~450,000 ha), which represent 5% of the country's surface and 11% of the forested area [16], the application of these methods is crucial. On the other hand, almost 50% of Cuba's surface area is dedicated to agricultural development, because it is a prioritized economic sector. However, runoff resulting from agricultural practices frequently flows into coastal mangrove forests, affecting these important ecosystems [17]. The GHNCA is also affected by the agricultural sector, in addition to the pollution associated with other socioeconomic activities. Although this PA extends across five municipalities (Chambas, Morón, Ciro Redondo, Bolivia, and Primero de Enero) of the province of Ciego de Avila, the mangroves of Morón are the most affected, due to higher levels of industrial development and health-related pollutants.

Furthermore, tourism development has also affected the region, particularly the northern keys of the province.

In recent years, there has been an increasing need to continuously monitor the structural and physiological changes occurring in mangrove forests, using appropriate ways to conserve them at minimal economic and temporal costs [18].

Kuenzer et al. [19] conducted a comprehensive review of mangrove ecosystem research using remote sensing techniques. In their analysis, they highlighted both the potentialities and limitations of this methodology, emphasizing especially the advantages it offers for the study and monitoring of these ecosystems. Despite the wealth of information available globally, it is important to note that in Cuba, research in this area is remarkably scarce [20]. This lack of studies limits our understanding of Cuban mangroves and their dynamics, as well as the ability to implement effective conservation and sustainable management strategies. Therefore, it is crucial to encourage research in remote sensing applied to mangroves in Cuba to take advantage of the opportunities that this technique offers.

One of the main problems with the effective management of the information provided by specialists in remote sensing methods is that it is a difficult process to learn for most people, sometimes tedious, and requires a high qualification to perform it [18,21]. For these reasons, WebGis-based platforms (which can be more accessible to decision makers) have been used for different purposes and spread around the world. Some researchers have built these platforms to support integrated coastal management activities [21,22], coral reef fisheries management [23], and mangrove forest management [24–26]. SIGMEM, as a WebGis tool, provides greater data transparency, versatility, comprehension, and ease of use by users inconsistent with the use of GIS and remote sensing techniques, in addition to improving the efficiency of data processing, which will allow rapid, accurate, and inexpensive monitoring of physiological and spatiotemporal changes in the mangrove forests of the GHNCA.

Limited studies of mangrove forests in the GHNCA confirm the need to introduce remote sensing techniques for their study and monitoring. Thus, the main objective of this work is to develop a web-based viewer that enables the assessment and understanding of the spatiotemporal variability of the mangrove forest dynamics. To achieve this, changes in deforestation, growth, etc., will be considered as experienced by the mangrove forests that can be evaluated from remote sensing data. The outputs of this application will provide a baseline for this important ecosystem, permitting spatiotemporal comparisons of the mangrove's health. This analysis also involves the attribution of mangrove health changes due to the influence of crucial hydrometeorological variables in the context of climate change, such as the mean sea level, temperature, precipitation, etc., as well as human-induced impacts that may lead to the need of more precise management measures.

2. Materials and Methods

2.1. Study Zone

The GHNCA is located in the province of Ciego de Avila, in the center of Cuba. It covers the territories along the marshy area near the coast (Figure 1), including parts from the municipalities of Bolivia, Primero de Enero, Morón, Ciro Redondo, and a small part of Chambas [27,28]. In the territory of Morón, it includes sites of ecological interest, such as the natural lagoons of La Leche and La Redonda, and extends to the marshy area near the mouth of the Chicola channel also including the Coco and Guillermo keys. It is bordered to the north by the Old Bahamas Canal; to the south by the Morón groundwater basin and the surface basins of the El Calvario, Naranjo, Robles and Cimarrones rivers, La Yana and several sub-basins of drainage canals that flow into the wetland; to the east by the Caonao River basin; and to the west by the Chambas River basin. The GHNCA has a surface area of 686.59 km^2 not including the northern keys [27,28]. Overall, the area extends about 40 km inland from the Big Island, covering most of the coast, the immediate maritime zone, and adjacent cays in this area.

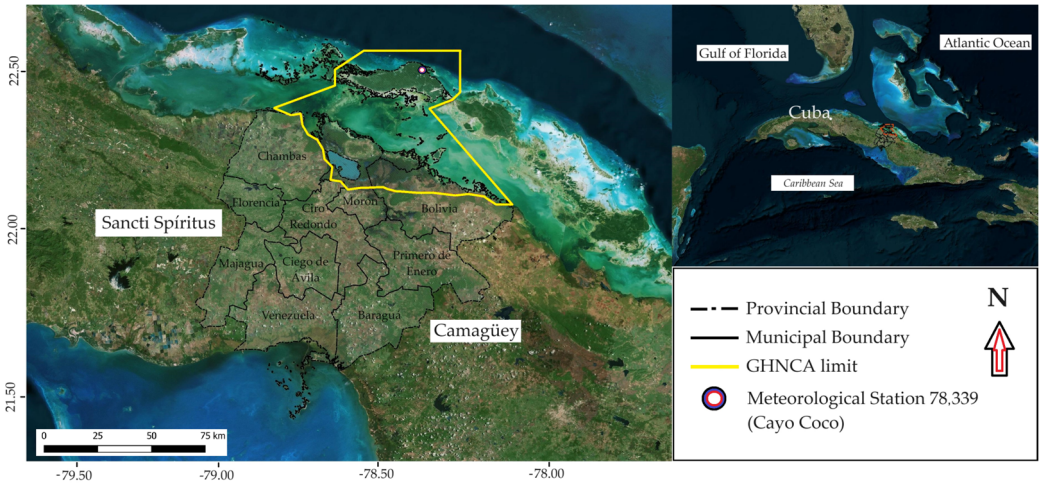

Figure 1. Location of the Gran Humedal del Norte de Ciego de Ávila (GHNCA), Cuba.

The precipitation regime of the GHNCA, like the rest of the country, is characterized by two annual periods, a rainy one from May to October and a dry one from November to April. Based on data from the Cayo Coco meteorological station, located within the limits of the GHNCA, the climatological values of some atmospheric variables were calculated. The annual average temperature is 26.1 °C. The coldest month is January with an average temperature of 23.4 °C, while the hottest month is July, averaging 28.6 °C. The average annual rainfall oscillates around 1574.0 mm, with minimum values ranging between 32 and 91 mm during the dry period, and the highest accumulated rainfall is October, with 165.8 mm. More information regarding the climatic conditions can be consulted in Gómez-Martín et al. [29].

Other studies also inform other characteristics of the study area, such as the description of the physical–geographical characteristics, flora, and fauna [30]; the status of hydrochemical water quality [31]; the diagnosis of the hydrological situation of the area; and the management of the wetland's waters to minimize its effects [28].

A spectral analysis of vegetation indices for mangrove forests in Cuba showed that the GHNCA stands out, only behind the Cienega de Zapata Wetland, for its vegetative dynamics and extent of mangrove areas [20]. These serve as habitat for a high fauna that makes the GHNCA stand out at a national level [32]. However, the mangroves of the GHNCA are vulnerable not only to hydroclimatic changes and extremes, but also to anthropic action. The Jardines del Rey archipelago, which is part of the GHNCA, has been exploited for tourism purposes since the 1990s. The prospecting and exploitation of new keys is still ongoing; together with urbanization, there has been deterioration of natural areas and esthetic degradation of the rural landscape, affecting their biological diversity [33]. In the GHNCA, hydrotechnical works have been inserted for socioeconomic interests, and specifically for tourism, so water exchange works have had to be carried out to promote the development of the mangrove ecosystem associated with the wetland [34,35].

This study was performed following the steps shown in Figure 2. The main elements of this flowchart are described in the subsequent sections, namely, "Training, Validation, and Selection of Optimal Classification Model" (Section 2.2); "Obtaining Cloud-Free Image Compositions and Spectral Indices" (Section 2.3), and "Publication of Geospatial Data as a Web Service" (Section 2.4).

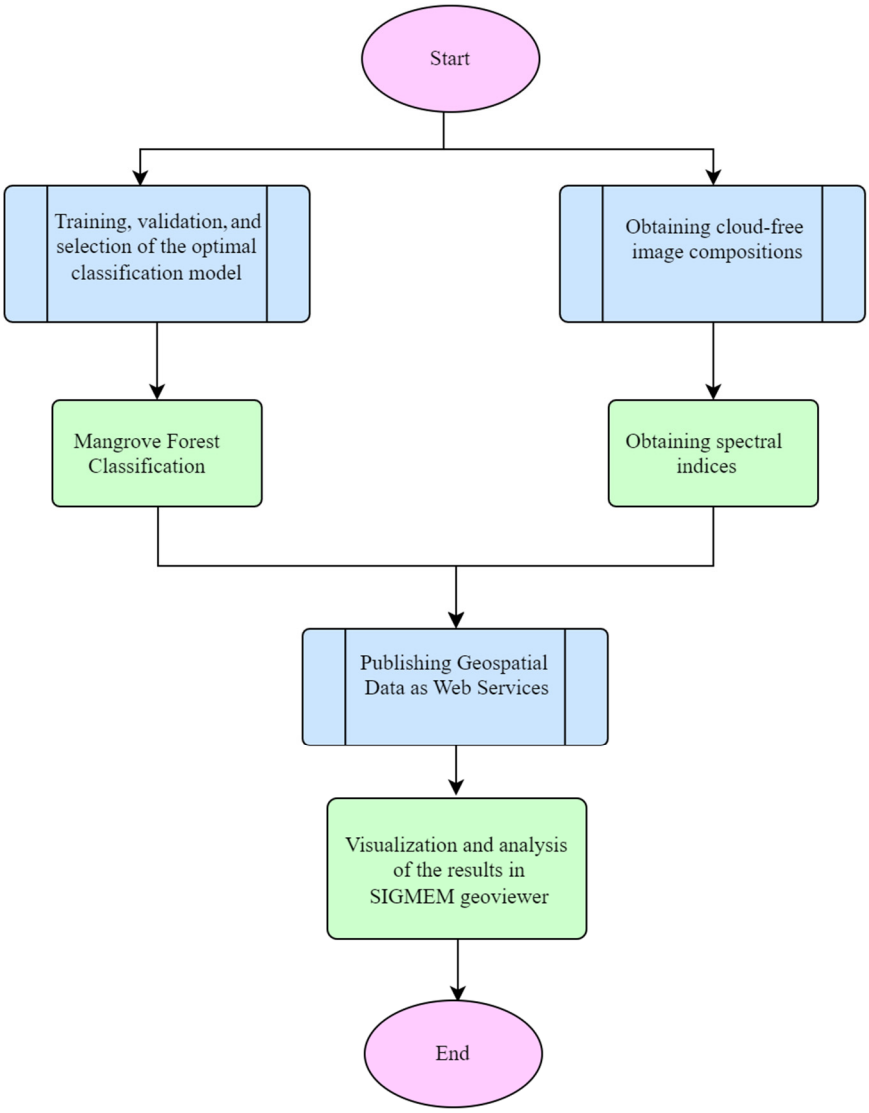

Figure 2. General workflow for the development of the WebGis platform: SIGMEM.

2.2. Training, Validation, and Selection of Optimal Classification Model

This section describes the field and satellite data used for training and validation of the classification algorithms, as well as the specific classification process carried out to select the most optimal classifier.

2.2.1. Satellite Data

To map the spatial distribution of the mangrove ecosystem in the GHNCA, we used Sentinel-2 surface reflectance level 2A (MSI) products (Table 1) [36], which were geometrically corrected to WGS 84/UTM zone 17N, eliminating the need for radiometric or geometric correction. Mangrove ecosystems show little spatial and structural variation over a year [37–39]; it was therefore decided to compose annual images for the corresponding period between 2020 and 2023. Images with a cloud percentage lower than 30% were selected, and a cloud mask was initially applied from the "QA60" band, which stores the cloud cover information. Afterward, a second filter was applied using the Scene Classification Map (SCL) product for eliminating pixels with values equal to 0, 1, 3, 8, 9, 10, and 11 (no data, saturated or defective pixel, cloud shadows, cloud medium probability, cloud high probability, thin cirrus, and snow or ice). The median of each of the spectral bands was then calculated, obtaining annual cloud-free images for the study area. The spectral bands of the visible (blue (B), green (G), and red (R)), red edge (Red.edge 1, Red.edge 2,

and Red.edge 3), near-infrared (NIR, nNIR), and shortwave infrared (SWIR1 and SWIR2) regions were selected. All bands were resampled to a spatial resolution of 10 m, and 50 spectral indices used in the classification model were retrieved from the selected bands. The entire process was developed on the Google Earth Engine (GEE) cloud computing platform [40,41].

Table 1. Spectral and spatial characteristics of the MultiSpectral Instrument (MSI) sensor aboard the Sentinel-2 mission.

S2A Bands	Central Wavelength (nm)	Bandwidth (nm)	Spatial Resolution (m)
B1 (Coastal aerosol)	442.7	21	60
B2 (Blue)	492.4	66	10
B3 (Green)	559.8	36	10
B4 (Red)	664.6	31	10
B5 (Red.edge 1)	704.1	15	20
B6 (Red.edge 2)	740.5	15	20
B7 (Red.edge 3)	782.8	20	20
B8 (NIR)	832.8	106	10
B8a (nNIR)	864.7	21	20
B9 (Water vapor)	945.1	20	60
B10 (Cirrus)	1373.5	31	60
B11 SWIR 1	1613.7	91	20
B12 SWIR 2	2202.4	175	20

2.2.2. Reference Data

The GHNCA survey began in 2020. Each month, georeferenced points were located with a Topcon HiPer SR precision GNSS receiver. From 2020 to 2023, the cover class (mangrove/non-mangrove) was identified at each of the points, placing greater emphasis on the areas occupied by mangrove varieties. The sampling points were homogeneously located over the entire study area. Due to difficult access in some regions, it was necessary to locate some points using visual interpretation of Sentinel-2 images. To distinguish mangrove-covered areas from the rest of the vegetation in the study area, the following band combinations were used: (i) NIR-Red-Green and (ii) SWIR1-NIR-Red. In the first combination, the mangrove can be clearly differentiated from the rest of the vegetation because the mangrove appeared in the image as a dark red and the rest of the plant species appeared as light red. In the second combination, the regions covered by mangrove appeared as a more intense green, while the rest of the vegetation appeared as a lighter green. A total of 5517 reference points were identified, with 2781 of them classified as "mangrove" class and 2736 as "non-mangrove" (Figure 3).

2.2.3. Obtaining Spectral Index

According to Gilabert et al. [42], a vegetation index can be defined as a parameter derived from the reflectivity values at different wavelengths, designed to extract information related to vegetation while minimizing the influence of disturbances such as those caused by soil and atmospheric conditions.

These indices exploit especially a peculiar behavior presented by vegetation in the red and near-infrared regions [8,9]. In this context, the present study utilizes various vegetation indices to analyze biophysical variables within the mangrove ecosystem of the study area. These four indices used are the Normalized Difference Vegetation Index (NDVI), Enhanced Vegetation Index (EVI), Canopy Level Chlorophyll Content Index (CCCI), and Normalized Difference Moisture Index (NDMI). The NDVI is calculated as the normalized difference between the red and near-infrared bands, ranging from (1) to (−1). This index, proposed by [43], is particularly susceptible to soil influence and has become the most widely used

in remote sensing [8]. Its calculation is very simple to implement, as evidenced in the following equation:

$$NDVI = (B8 - B4)/(B8 + B4) \quad (1)$$

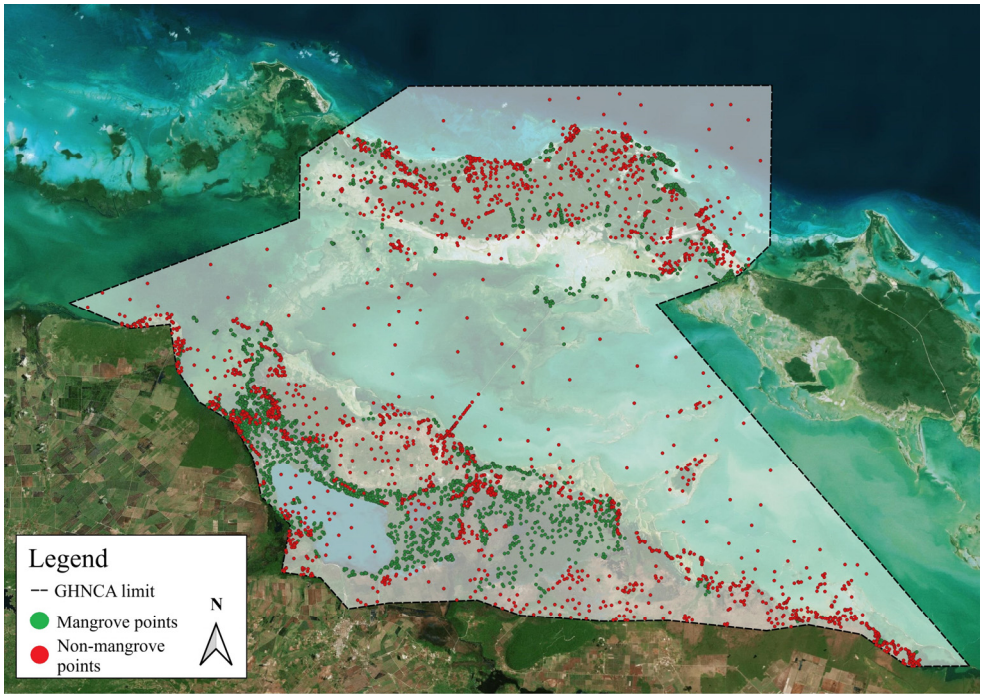

Figure 3. Spatial distribution of the reference points taken in the GHNCA. Green dots indicate mangrove class and red dots non-mangrove.

EVI, like NDVI, is related to the fraction of photosynthetically active radiation intercepted by vegetation [44]. It is aimed at improving sensitivity to differences in vegetation cover and providing a more accurate measurement of vegetation density in areas where vegetation is dense. Its formulation is described below as follows:

$$EVI = 2.5 \times ((B8 - B4)/(B8 + 6 \times B4 - 7.5 \times B2 + 1) \quad (2)$$

The CCCI has an indicator function of plant health and primary productivity, being considered the most relevant plant property for the estimation of productivity [45].

$$CCCI = ((B9 - B5)/(B9 + B5))/((B9 - B4)/(B9 + B4)) \quad (3)$$

The NDMI [46] relates the SWIR1 shortwave infrared band of the Sentinel-2 satellite to the green band of the same satellite. The formulation for this index is as follows:

$$NDMI = \frac{B8 - B11}{B11 + B8} \quad (4)$$

2.2.4. Classification Process

To perform the mangrove forest classification, the reference observations collected between the years 2020 and 2023 in conjunction with Sentinel-2-derived spectral data (B2–B8A and B11–B12) and the vegetation indices calculated were pooled into one database. With this, we ensured data consistency, better representation of classes to capture temporal and spatial variations, and a larger database, which allows for efficient training of robust models, such as RF. A total of 80% and 20% of the data were used for training and validating the results, respectively. These were generated by stratified random partitioning based on the number of reference points with mangrove/non-mangrove to ensure the same proportion of both cover classes in both sets. In the training set, 4413 observations were pooled

(2250 mangrove and 2163 non-mangrove), and in the validation set, 1104 observations were distributed in 531 of the mangrove class and 573 of the non-mangrove class. The CARET library [39–41] was used to perform this.

The automated classification process for mangrove forest mapping is oriented within the geovisor process flow using GEE. However, one of the main drawbacks encountered in the classification processes in GEE is the inability to adjust the hyperparameters required in each of the implemented algorithms [47]. To overcome this, the classification procedure was carried out using R statistical software version 4.2.3 [48] to then use the optimal model in GEE. From the group of existing algorithms within the GEE platform, Random Forest and Naive Bayes were selected, following the criterion of evaluating a non-parametric and a parametric algorithm on our dataset. The methodology and results provided by RF and Bayesian networks are easier to understand in comparison to neural networks, which are considered as "black boxes" because it is hard to figure out how they actually make their decisions. The implementation of other techniques such as Support Vector Machines, is also a challenge, as their results are also difficult to interpret, particularly the uncertainties, whereas NB and RF models are more effective in this point. Random Forest (RF) is a non-parametric algorithm that constructs a set of randomly grown trees, where the predictions of individual trees are subsequently aggregated [49,50]. The Naive Bayes (NB) algorithm, on the other hand, is a parametric algorithm based on the Bayes theorem with the "naive" assumption of conditional independence between each pair of features given the class variable [51].

Before training the classifiers, selecting the most influential spectral indices and discarding the weak features was required. For this step, the model-based recursive variable elimination method [52] was used, employing the RF model with a bootstrapping resampling method with 10 repetitions. From the "top" of 10 spectral indices, the three most important ones were selected, because from the third predictor onward, the improvement was minimal: (i) NDVI [53], (ii) RDVI [54,55], and (iii) NDWI [56]. The starting model consisted of the 10 spectral bands and the three selected indices (Figure 4).

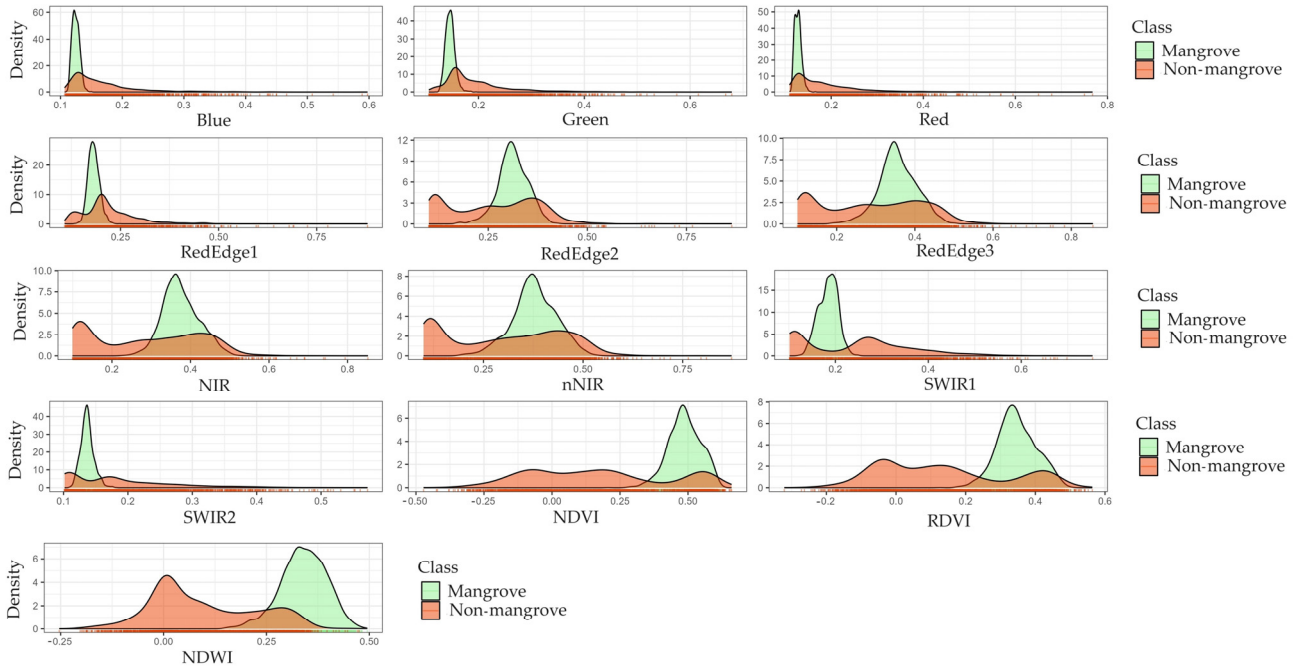

Figure 4. Distribution of predictor variables used in the classification model grouped by classes (mangrove/non-mangrove). Selected Sentinel-2 spectral bands and spectral indices selected by the recursive variable elimination method.

The optimization of the classifier hyperparameters was performed by randomly searching the parameter space of the training data by sampling 10 random combinations. To carry on the following evaluation, a cross-validation (CV) with three replicates was implemented. By optimizing the hyperparameters and evaluating the model on multiple subsets, a balance between fit and generalization is sought. This reduces the risk of overfitting the model to the peculiarities of the training data.

The classification accuracies of each machine learning algorithm were evaluated using the confusion matrix [57,58] and the Kappa statistic [59]. Afterward, the overall accuracy (OA, in %), F1 scores [60,61], user and producer accuracy, and errors of omission and commission were calculated from the confusion matrix [62]. The estimated results and overall performance of the classifiers were further evaluated using McNemar's [63,64] two-tailed non-parametric statistical test at a confidence level of 95%. McNemar's test is based on the calculation of the X^2 distribution and is commonly used to compare the classification errors between two classifiers. We considered a statistical difference when the values of McNemar's test exceeded 3.84, with a confidence level of 95% [50,65].

2.3. Obtaining Cloud-Free Image Compositions and Spectral Indices

Spectral vegetation indices (VIs) have been used in the field of remote sensing since the early days of remote sensing as an indirect way of estimating biophysical vegetation variables [66]. These indices, based on remotely sensed data, exploit the high contrast between the red and near-infrared (NIR) bands of vegetation [53]. Optical images derived from satellite remote sensing are used to estimate VIs. During the evaluation of their usability, it is essential to consider the cloud cover present in the scenes. The processes described in this section were incorporated within the general flow (right branch of Figure 2) and, as can be seen, their execution, with a quarterly frequency, is independent and parallel to that of the classification. All geospatial analyses related to cloud masking, image compositing, and spectral index calculations were conducted using GEE. This platform combines a catalog of several petabytes of satellite imagery, along with geospatial datasets with planetary-scale analysis capabilities. In addition, it is free to use for academic and research purposes.

Obtaining Cloud-Free Image Compositions

The presence of clouds in the scene produces alterations in the surface reflectance (SR) measurements and the derived magnitudes such as the vegetation indices and digital canopy classification. In addition to clouds, shadows cast by clouds also invalidate the use of the data in certain regions of the images. Consequently, detecting clouds and their associated shadows is a crucial processing step in the preprocessing of optical images. These tasks have been deserving of extensive research efforts by the scientific community [67].

The COPERNICUS/S2_CLOUD_PROBABILITY collection was used for cloud detection and masking in this work [68]. These images have a single band called "probability" whose values are distributed from 0 to 100, indicating the probability that the pixel is covered by clouds. The generation of the images of this collection is performed using the Python (v3.12.7) library called s2cloudless. This algorithm was developed by the EOResearch team at Sinergise and is published under the MIT license on https://github.com/sentinel-hub/sentinel2-cloud-detector (accessed on 9 October 2024). The effectiveness of this algorithm is discussed in a comparative study [69] conducted as part of the Cloud Mask Intercomparison eXercise (CMIX), where the performance of several algorithms for cloud detection was evaluated using a standard set of different metrics, derived from the following confusion matrices: Overall Accuracy (OA), Balanced Overall Accuracy (BOA), Producer Accuracy (PA), and User Accuracy (UA). The S2cloudless algorithm, specifically, was contrasted on four datasets: CESBIO, GSFC, Hollstein, and PixBox (https://calvalportal.ceos.org/cmix-sites, accessed on 9 October 2024). The average result for the accuracy of the S2cloudless algorithm in each of the metrics was OA = 89.02, BOA = 88.77, PA = 84.5, and UA = 94.9. This algorithm obtained the best accuracy in terms

of the relationship between the PA and UA metrics. According to the CMIX results, the greatest difficulties are found in the detection of thin and semi-transparent clouds, which is a common problem for current cloud detection algorithms. These datasets capture the spatial and temporal variability necessary to characterize the effectiveness of the proven cloud detection algorithms and, in particular, S2cloudless, so it can be assumed that the results of the metrics are generalizable and applicable to the spatial and temporal environment of the study area.

The optical images used were those corresponding to the COPERNICUS/S2_SR_HARMONIZED collection [70]. Each image in this collection has 12 spectral bands that represent the SR scaled by 10,000. There are also several bands more specific to the L2 processing level. In addition, there are three quality control bands present, where one (QA60) is a bitmask band with cloud mask information created under spectral criteria [71].

The process began by filtering the data from the COPERNICUS/S2_SR_HARMONIZED and COPERNICUS/S2_CLOUD_PROBABILITY collections by date and region of interest. To ensure that the percentage of cloud-covered pixels (CLOUDY_PIXEL_PERCENTAGE) did not exceed a predetermined threshold (CLOUD_FILTER), an initial filter was applied to the first collection.

From the resulting images, a new collection was created by combining the matching images in the "system:index" field. Afterward, a new band called "s2cloudless" that contains information about the cloud cover probability is added to each image of the first collection. In this band, the "probability" band is compared with the previously set threshold (CLD_PRB_THRESH). Finally, a "probability" band is added to the processed image, together with another band labeled "clouds" if the CLD_PRB_THRESH value exceeded the "probability" value.

It is important to detect and mask shadow zones produced by clouds in addition to identifying the clouds themselves. To achieve this, we utilized the spectral properties of the NIR band. In this case, surface radiance values are compared with a previously established limit. Water bodies exhibit a spectral behavior similar to the shaded areas, so it is necessary to previously disregard these regions in the analysis. The above procedure returned areas with low levels of surface radiance that are visually characterized as dark pixels.

The projection of a cloud's shadow must be projected in the same direction as the sunlight incidence. This assumption is used as a criterion to accurately identify and select areas that are truly covered by cloud shadows. To apply this criterion, the most probable direction and distance of the shadow's projection in the UTM (Universal Transverse Mercator) system is determined. The sunlight incidence direction data are accessed through the "MEAN_SOLAR_AZIMUTH_ANGLE" property of the images. The potential shadow projection area is intersected with the dark pixels of the image and added as an additionally labeled "shadow" in the processed image.

Finally, using the shadow and cloud band values, we created a binary mask band in which pixels belonging to these classes are assigned a value of 1, while the rest are assigned a value of 0. As a complementary task, very small cloud or shadow areas are eliminated and the rest of the areas are dilated to obtain more homogeneous regions. Following the previous procedure, the mask layer is applied to each band of the images to eliminate those regions with a high probability of being covered by clouds or shadows.

During a three-month analysis period, an image is generated by calculating the median of all images taken during this period. This process includes the detection and masking of shadows and clouds, resulting in a final composite image that is free of any clouds or shadows.

2.4. Publication of Geospatial Data as a Web Service

A service oriented toward web architecture was developed to enable access to the information obtained through the above-mentioned procedures. It was achieved using open-source technologies such as MapStore, Geoserver, Django, and PostgreSQL with its

Postgis extension. These technologies allowed for technological independence during the development of the work.

To ensure interoperability, international standards of the Open Geospatial Consortium (OGC) were used for the exchange of geographic information. Figure 5 provides a conceptual diagram of the web architecture employed.

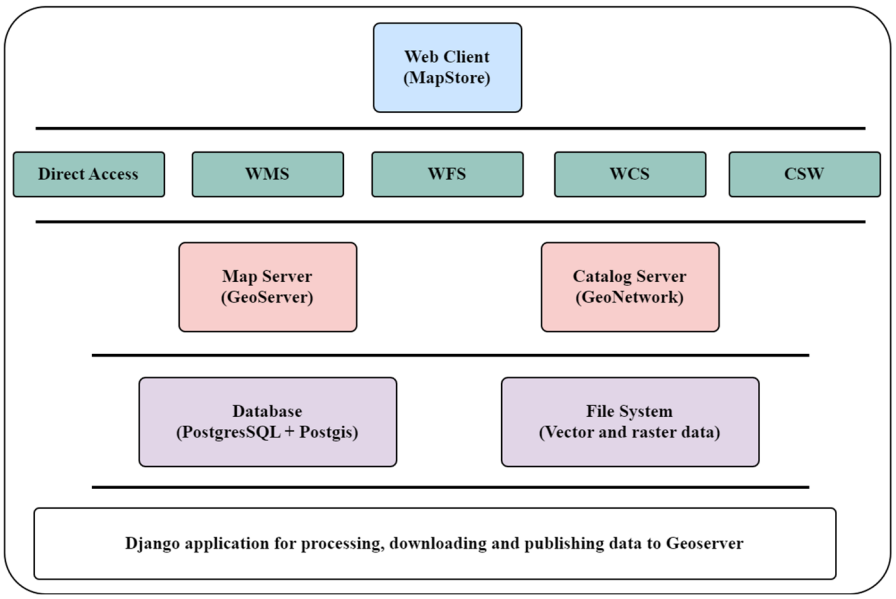

Figure 5. Diagram of the web architecture used for the development of the GeoServer.

A web server was implemented using the Django framework for automating and programming the algorithms. PostgresSQL is the database engine utilized, with its Postgis spatial analysis support extension. GeoServer is used as the map server, which consumes data from both PostgresSQL and the server's local file system. The data are indexed using metadata through the GeoNetwork metadata server and offered to users through a web application called MapStore. The web interface accesses the Geoserver data through the use of standards for the exchange of geographic information, including Web Map Service (WMS), Web Feature Service (WFS), Web Coverage Service (WCS), and metadata through Catalogue Service Web (CSW) offered by GeoNetwork.

The preprocessing and processing algorithms are performed from the Python client library for GEE, earthengine-api. These algorithms are sent to be executed from the server to the GEE platform after the authentication process is completed. Once the results of the procedures are obtained, the resulting data are downloaded to the server's local file system and sent for publication in GeoServer.

The introduction and publication of data in GeoServer are performed through the use of the REST API (Representational State Transfer Application Programming Interface). This API allows clients to manage GeoServer without accessing the web administration interface. The Python library used for these functions, named geoserver-rest, enabled the creation, updating, and deletion of work areas, stores, layers, and styles. This allowed for the publication of the data according to OGC standards, guaranteeing its subsequent consumption by any authorized client.

Workflow Automation

One of the most outstanding elements of the developed architecture is the automated workflow, which comprises the stages of data preprocessing, processing, downloading, and publishing. The entire process is managed by scheduling tasks that are executed asynchronously using Celery. Celery is an open-source tool used for real-time task management [72,73] and is fully integrable with the Django framework.

Four tasks with specific, well-established objectives were programmed within the framework of the project:

1. Obtaining a composition of cloud-free images of the study area;
2. Obtaining spectral indices;
3. Downloading data in GeoTIFF format to the project's Google Drive folder using the Python PyDrive2 library;
4. Introduction of the images to GeoServer using the Python library geoserver-rest.

The general workflow executed the scheduled tasks at two specific points in time. The components of the classification flow proposed in Section 2.2 are executed every 12 months. On the other hand, the tasks of the workflow proposed in Sections 2.3 and 2.4 are executed every three months. Tasks are configurable through the use of the Django administration interface. A record is kept of the dates on which the tasks were executed, and the execution interval is controlled by entering a timeout. This timeout is checked every 24 h by an automatic process and is measured from the last execution time of the tasks.

We used the Python programming language to develop the proposed platform, and the following libraries and frameworks for the execution of the different stages:

- earthengine-api: client library used for the execution of algorithms on the GEE platform;
- PyDrive: library for managing the Google Drive storage space corresponding to the GEE project;
- geoserver-rest: client library for GeoServer management without the use of the user interface;
- Django: a framework for developing web applications and scheduling automatic execution tasks.

At the end of each execution cycle, it is possible to retrieve from the client platform the information processed and published in GeoServer. This guarantees the availability of the updated information within the established period.

3. Results

3.1. Mapping Mangrove Ecosystems with Sentinel-2 Imagery

The model combining spectral bands and selected spectral indices using the recursive elimination method trained with RF proved to be the most efficient in classifying mangrove-occupied areas (Table 2). The OA obtained with RF was 94.11%, with a PA > 95%. The Kappa and F1 values obtained with RF were also very satisfactory (0.94 and 0.90, respectively). Although inferior to those obtained with RF, the OA value achieved with NB was 89.85% and the BP for the target class was above 90%. The Kappa values and F1 score achieved by the NB classifier were 0.86 and 0.80, respectively.

Table 2. Overall accuracy results for Random Forest and Naive Bayes classifiers. Producer accuracy (PA) values for the Mangrove class and overall accuracy (OA) are expressed in %. F1 score and Kappa statistic are shown. McNemar's comparison of classifier performances. Note: test values > 3.84 show that a statistical difference exists at the 95% confidence level.

Model	Algorithm	OA (%)	F1 Score	Kappa	PA (Mangrove) (%)	McNemar (RF vs. NB)
Spectral bands + spectral indices (NDVI, RDVI, NDWI)	Random Forest	94.11	0.90	0.94	96.16	4.12
	Naive Bayes	89.85	0.80	0.86	92.01	

The results of McNemar's test confirmed that the differences in classification performance between the two algorithms in the pairwise comparison (X^2 0.05 = 4.12) were statistically significant (Table 2). This result confirms that the overall accuracy of RF was significantly higher than the accuracy obtained with NB.

After evaluating the classifiers and selecting the optimal one for mapping the areas occupied by mangroves in the GHNCA using the R environment, we migrated to the GEE

free platform and determined the occupied areas for each year from 2020 to 2023. The largest estimated areas were for 2020 and 2021 with 27,239.86 and 27,811.30 ha, respectively, followed by 2022 with 24,408.10 ha and 2023 with 22,101.69 ha (Figure 6). However, the differences in estimated areas across these years are not statistically significant ($p > 0.05$). Although the difference between the estimated areas of mangrove ecosystems in the GHNCA is not statistically significant, a decreasing trend is observed (Table 3). The net change calculated based on the year 2020 shows a decrease of 5138.17 ha (−2.10%) in the year 2023 and in the year 2022 a decrease of 2831.76 ha (−1.16%). These annual changes can be analyzed automatically using the viewer, as well as the changes in the health status of this ecosystem within the mapped areas.

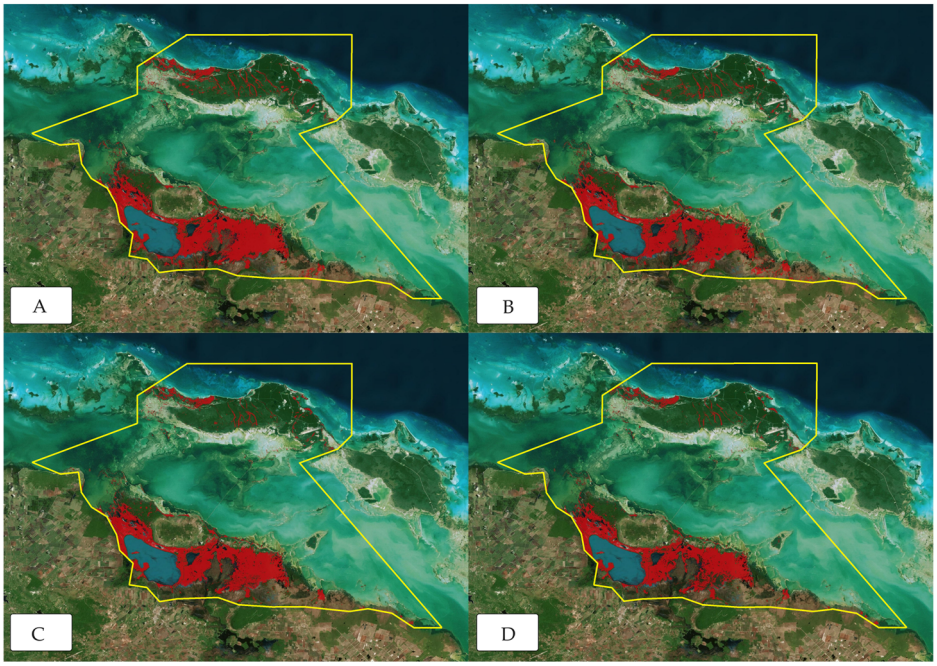

Figure 6. Estimated mangrove areas in the GHN in Ciego de Avila, Cuba emulating Sentinel-2 images. (**A**) 2020, (**B**) 2021, (**C**) 2022, and (**D**) 2023. Legend: the areas occupied by mangrove ecosystems in each of the years are shown in red; the limits of the GHN of Ciego de Avila are shown in blue dashed lines.

Table 3. Mangrove proportions for each year in hectares (ha) and percentage of total area. Overall net mangrove changes in hectares (ha) and in percent (%), with 2020 being the base year.

Year	Area (ha)	% of the Total Area	Net Change (ha) Compared to 2020	Net Change (%) Compared to 2020
2023	22,101.69	9.03	−5138.17	−2.10
2022	24,408.10	9.97	−2831.76	−1.16
2021	27,811.30	11.36	571.47	0.23
2020	27,239.86	11.13	-	-

3.2. Web Geoviewer of the Great Wetland of the North of Ciego de Ávila

The development of the present work contributed fundamentally to generating the data and developing the computer architecture necessary for the implementation of a geovisor (Geospatial System for the Monitoring of the Mangrove Ecosystem or SIGMEM) for the GHNCA. All the components that make up the computer architecture of the system are deployed using Docker, a technology that allows an efficient deployment and scaling of computer applications, with minimal resource consumption, among other benefits.

Figure 7 shows an image of the client application of the SIGMEM geovisor. This component allows users to access essential functions of analysis such as the search, visualization, and downloading of geographic information. The security is guaranteed for each user through the use of access credentials. In this case, the WebGIS application used is MapStore.

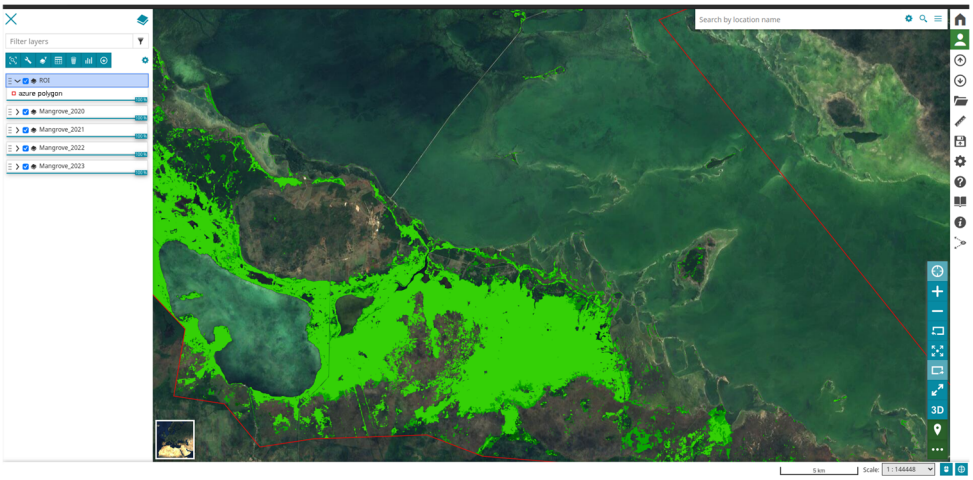

Figure 7. Two-dimensional view of the workspace within the MapStore application. The red line represents the limit of the GHNCA.

Users have several options, including the execution of measurements, downloading and loading of layers to and from different data sources, respectively, manipulating styles and other visualization elements, and querying of layer attributes. Figure 8 demonstrates that a prominent feature is the possibility of visualizing loaded data in 3D, provided that they have elevation attributes or are provided in a relevant format.

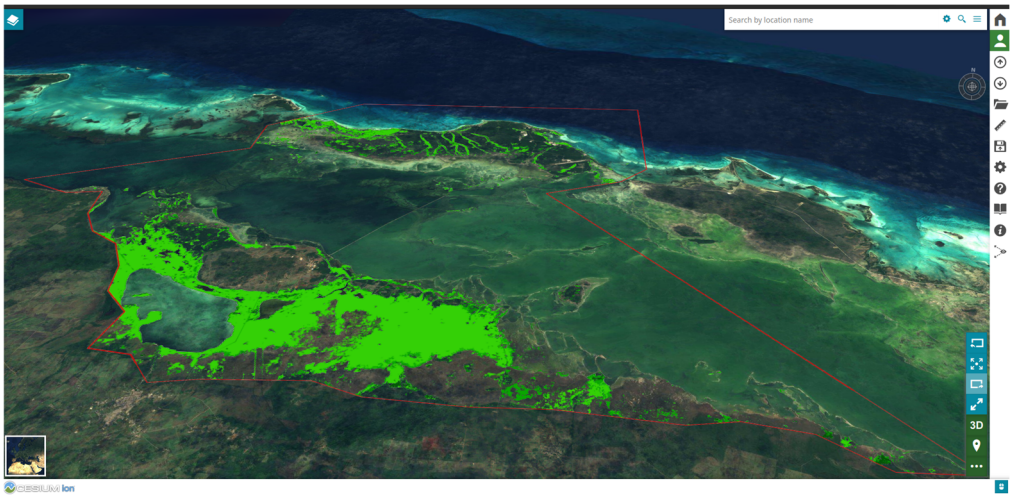

Figure 8. Three-dimensional view of the workspace within the MapStore application. The red line represents the limit of the GHNCA.

The implemented web client includes a metadata catalog service accessible from the SIGMEM interface, allowing users to search and add layers to the map composition. Figure 9 shows an example of the data available on the map server, which can be accessed through the metadata tab of each resource.

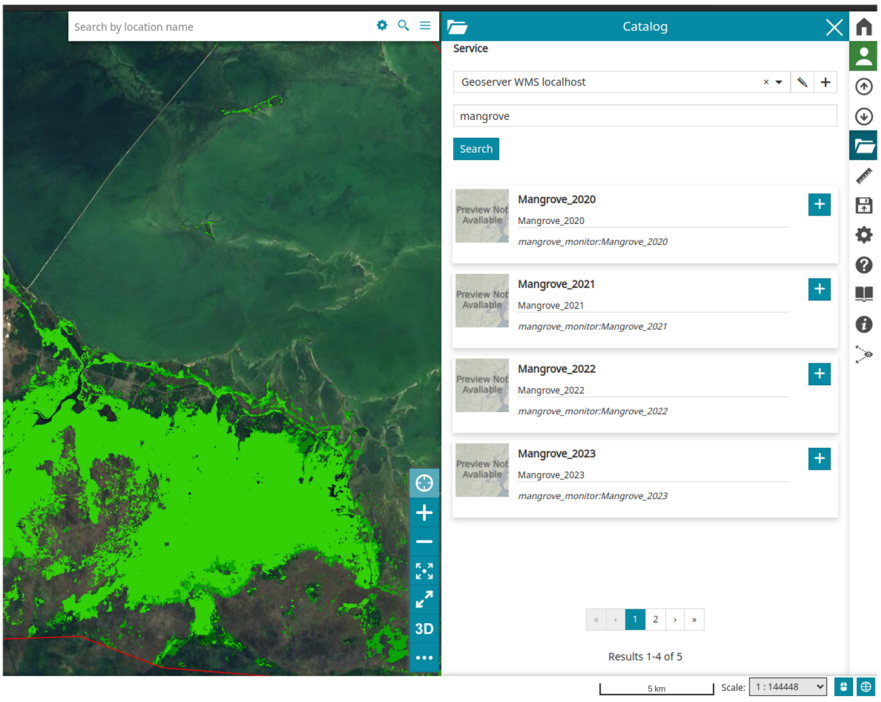

Figure 9. Access to the metadata catalog of geospatial resources. The red line represents the limit of the GHNCA.

The layer comparison feature, characterized by a horizontally sliding bar that controls the display of the selected layer, allows the visual inspection of the differences between two different datasets. Figure 10 shows an example of the comparison between the classification results for the years 2020 and 2021.

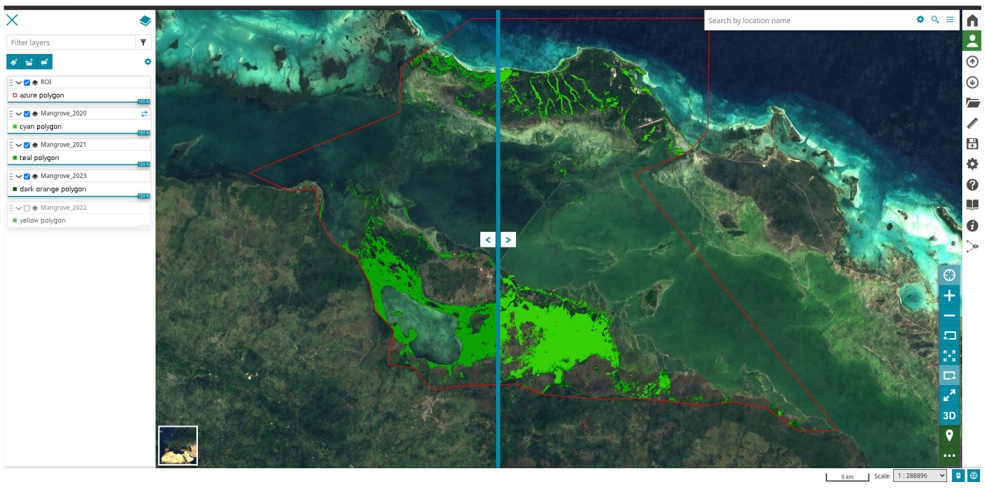

Figure 10. Functionality for visual intercomparison of layers. The red line represents the limit of the GHNCA.

Other benefits of the web client concerning layer attributes include the editing, filtering, localizing by selection, and plotting. Figure 11 illustrates, in the lower region, the table of attributes and the tools for the manipulation of these attributes.

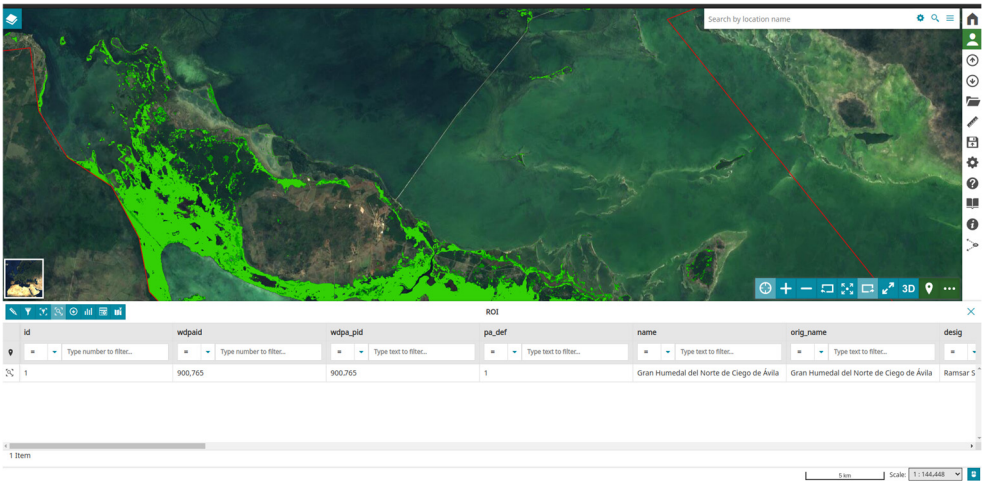

Figure 11. Features for viewing and manipulating layer attributes. The red line represents the limit of the GHNCA.

The composite image in Figure 12 shows the calculated indices for the July–August–September quarter of 2023. The data are managed through the metadata service and subsequently added as layers to the web map from GeoServer. Note that each of these layers includes a legend that ensures the understanding of the symbology used to represent the value of the calculated indices. The symbols are assigned from the map server using the Styled Layer Descriptor (SLD) markup language.

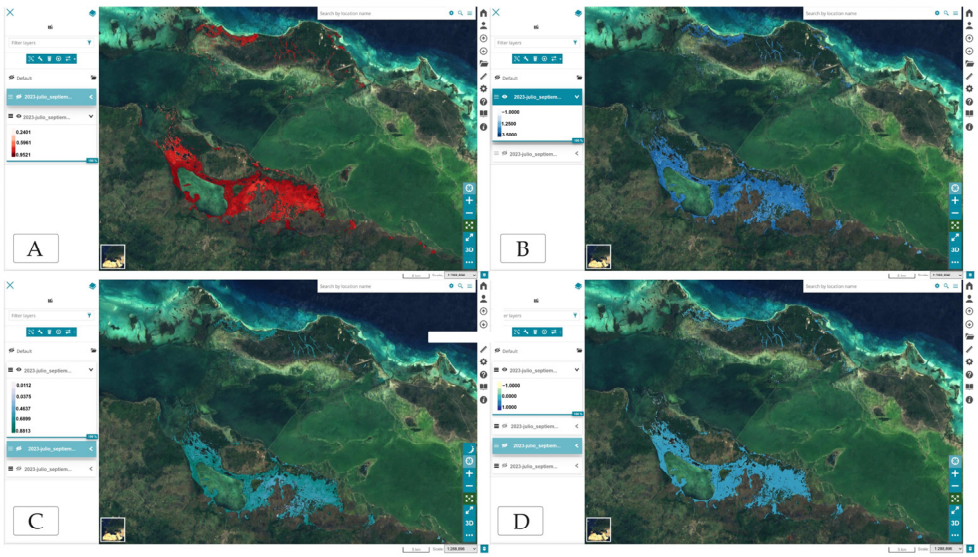

Figure 12. Vegetation Indices calculated in the GHN of Ciego de Avila, Cuba during the third quarter of the year 2023 emulating Sentinel-2 images. (**A**) NDVI, (**B**) EVI, (**C**) NDMI, and (**D**) CCCI.

4. Discussion

The current research introduces a web-based viewer (SIGMEM) that for the first time permits an assessment of the changes in mangroves within a specific area in Central Cuba. The evaluation incorporates spatial and temporal variations based on various vegetation indices. The use of Sentinel-2 images in this work, with a spatial resolution of 10 m, is sufficient for a regional scale analysis, as they maintain spectral resolution that allows the calculation of broadband indices, which are highly correlated with biochemical and structural plant parameters [74,75]. Hamilton et al. [76] obtained a global scale map of mangrove ecosystems using this type of imagery, and the results have been successfully applied in international mangrove assessment programs.

The results obtained in mapping the mangrove ecosystem coverage in the GHNCA using annual composites of Sentinel-2 satellite images were considered satisfactory, achieving an OA of 94.11%, which is superior to results obtained in other mangrove mapping studies [77–79]. Of the two algorithms evaluated for mangrove ecosystem mapping (RF and NB), RF demonstrated superior performance compared to NB (Table 2). RF achieved a higher PA value for the target class (mangrove) with 96.16% (lower error of omission), which is 4.15% higher than the PA obtained with the NB classifier. Similarly, when comparing the OA, F1 score, and Kappa values, we observed that RF was superior to NB in discriminating between the mangrove and non-mangrove classes, with an OA of 94.11%, an F1 score of 0.90, and a Kappa of 0.94. With NB, the obtained OA values for these metrics were 89.85%, 0.80, and 0.86, respectively.

Along the lines of classification for mangrove ecosystem mapping, both the RF and NB algorithms have been widely used [78,80–87]. Consistent with the results achieved in this study, various studies [79,88] have observed a superior performance of RF in mapping regions occupied by mangrove ecosystems. These results indicate that the best algorithm to use for mapping the areas occupied by mangroves in the GHNCA is RF. This conclusion was supported by the results of McNemar's non-parametric test in the pairwise comparison between classifiers, with an X^2 0.05 = 4.12 (overall accuracy of RF significantly higher than that of NB).

In many remote sensing investigations, hundreds of indices have been applied, while in our case, the number was limited to four (NDVI, EVI, CCCI, and NDMI). The selection of the indices was made considering their characteristics and their previous applications in mangrove studies [89–102].

The characterization of the indices was conducted considering mangroves as simple vegetation cover; however, a mangrove forest is more complex. Its distribution is not homogeneous, with the presence of fragmentations and patches of trees with different characteristics (age, degree of development, and species composition), as well as the presence of other types of vegetation [103]. This high heterogeneity generates a wide dispersion of spectral values. Nevertheless, a satisfactory level of precision would be achieved by comparing the distributions of the same index between different sites within the area, while the comparisons between indices also provides information on their properties. The indices also demonstrated a high relationship with forest cover density, which has been exposed as one of the disadvantages of many indices [99]. In their study, [104] obtained significant nonlinear relationships with the percent canopy cover for nine vegetation indices, including NDVI. A significant linear relationship offers an advantage for assessing the degree of vegetation cover; however, when projecting to describe other biophysical parameters, this becomes a difficult variable to assess.

Comparing the spectral patterns of mangrove forests with other forest types helps to corroborate the accuracy of vegetation indices for mapping studies. The combination of spectral responses to different combinations of vegetation indices can contribute to form a secondary spectral signature, which can jointly help to form a spectral library with practical value. This library would be useful for discriminating and identifying different vegetation formations. Despite this assertion, studies of the spectral signatures of different mangrove species are very scarce [105]. However, the use of spectral data should not be limited to observe and evaluate coverages and detect spatial and temporal changes [106]. Spectral information can be very useful for conservation-directed research [96].

The tasks performed during preprocessing may vary depending on several factors, such as the objectives pursued, the work methodology, and the primary data used. Bayo et al. [107] conducted a spatiotemporal study to detect changes in mangrove forest cover in Gambia over two decades (2000–2020) from Landsat imagery. There were three preprocessing stages in this study (creation of the multiband image, elaboration of the mosaic, and application of geometric corrections in the study area) and all were performed in ERDAS Imagine desktop software. In agreement with [108], the use of remote sensing-oriented desktop software (ERDAS, ENVI, eCognition, etc.) offers some challenges to overcome. The

first is that many of these software require a license for their use and must be previously installed, which can be cumbersome for some non-professional users. Secondly, there is a high time consumption in the processes of downloading and preprocessing large volumes of data on personal computers, which increases the complexity in proportion to the size of the area studied. These difficulties were overcome [108], as in this study, by using the GEE cloud computing platform. However, it should be noted that to use this platform, some basic programming skills in JavaScript or Python are required. Chen et al. [109] used GEE for the creation, from classification methods, of a mangrove forest map using, among other elements, the modified Normalized Difference Water Index (mNDWI). The initial data were extracted from optical images that were generated by Landsat 7–8 satellites and radar images produced by the Sentinel-1 satellite, between 2014 and 2016. In this work, the preprocessing is performed partly on GEE and partly on desktop software, mainly related to the preparation of the radar data.

One of the critical aspects is the treatment of images with clouds, which is a challenge, especially in regions that typically have high cloud cover. The authors of [110] found that a major difficulty for the study of the mangrove is the availability of images with low cloud cover. This issue is addressed in the present study by using algorithms for the masking and removal of areas covered by clouds or their shadows [67,69,111]. In addition, the spectral description of mangroves is not limited to the study area. This can be the starting point to use the output of this work in other studies, such as those related to monitoring the health status of these forests; for natural enjoyment in the context of tourism development; to evaluate their ecosystem value in the face of disasters; or conversely to assess the impacts received by hurricane incidences. Overall, the ability to study the dynamics of mangroves and other vegetation types will continue to improve as more advanced sensors and new algorithms for processing spectral data become available. SIGMEN is an initial version of a project that will be further improved. For instance, we plan to include recent metrics such as data from satellite observations of solar-induced chlorophyll fluorescence (SIF), which have opened up an opportunity to assess the seasonality of plant growth from the perspective of photosynthetic phenology [112,113]. This technique has even proven valid for distinguishing mangrove species rather than considering them as a whole, contributing to a better understanding of the photosynthetic mechanism of mangroves in subtropical and tropical wetland ecosystems.

The growing development of technologies such as WebGIS, understood as a Geographic Information System that takes advantage of web technology to communicate among its components [114], has had an impact on the way of studying phenomena whose best interpretation is sustained in a spatiotemporal framework. For example, Sukojo and Lisakiyanto [115] developed a WebGIS for early detection of potential forest fire outbreaks in a region of Sumatra Island. The authors described the use of tools such as a web server (XAMPP Control Panel), database manager (phpMyAdmin), and desktop Geographic Information Systems (GIS) (QGIS) for the conversion between formats and JavaScript web-mapping library (Leaflet). However, in the research report, there is no mention of the use of any map server, Geoserver in the case of this study, for the standardization of the data consumed by the client application.

The potential of cloud computing is reported by the authors of [116], who developed a workflow for loading satellite data, carrying out specific processes, and generating the desired products. This workflow implements a web viewer called Virtual Earth Laboratory (VLab) that allows monitoring of water stress in Europe, as a demonstration of its feasibility. All workflow results are stored in GeoServer, documented in GeoNetwork, and available through the WebGIS MapStore. This system, like SIGMEN, allows, among other benefits, the creation of control panels and personalized map compositions, which contributes to better visualization of the results for end users. All this technology is open-source, robust, and reliable, and its use is consistent, as is also observed in the study discussed here, which also incorporates the use of others such as Django, PyDrive2, and geoserver-rest.

Other technologies are employed by [117], this time focused on the development of a web-based flood risk information system called WebFRIS for a district in eastern India. This system is designed by using several open-source web tools and packages such as Google Maps, PHP, MySQL, and JSON. The strength of the aforementioned study is that the authors of the work pay attention to obtaining a friendly user interface design so that said system can be easily accessible to any end user, regardless of their technical knowledge. In this case, the use of open-source technologies, although different, is a point of agreement with the study presented here.

The present work contributes to the idea of automating workflows in the investigation of topics related to the spatiotemporal distribution of mangrove forests as a necessity in current research. It is in agreement with Giri et al. [118], who argue that it is essential to automate image preprocessing and processing tasks given the large amount of existing data. There is a tendency toward automation in the era of intelligence, which according to the taxonomy expressed by [114], is no longer oriented only to workflows to perform certain processes or execute algorithms, but also toward greater automation in the construction of ontologies that can then be used to generate knowledge and obtain information about specific application/business processes. The present work does not have this scope and is encompassed within the results obtained in the "cloud" era; however, recommended is the evolution of efforts toward the development of products that offer a higher level of usability among non-professional users, as described in the intelligence era [119].

The socioeconomic development of the Cuban archipelago has led to the implementation of various actions, mostly of an anthropic nature, which act as tensors on the functioning of the mangrove ecosystem to the detriment of its health [120]. The construction of roads and landfills for tourism infrastructure development (such as hotels and roads) in Cayo Coco has impacted the mangrove ecosystem. In the first case, portions of the forest have been enclosed, most of which have died due to increased salinity and the decomposition of organic matter. The landfills have buried areas of mangroves, leading to an irreversible loss [8]. Furthermore, tourism activities generate solid and liquid wastes (such as wastewater) that, if not properly managed, can contaminate mangrove areas, affecting their health and the biodiversity that depends on them [121]. Therefore, SIGMEN represents an ideal tool for monitoring the changes in vegetative dynamics of the mangrove forest in the GHNCA, which is crucial for the authorities in charge of its management. SIGMEN will allow monitoring of changes in the vegetative dynamics of the mangrove and will provide accurate information to the authorities in charge of its management for the subsequent identification of the agents causing the damage, thus contributing to decision making for the preservation of this ecosystem.

The results achieved in this study can be improved by incorporating procedures characteristic of the era of WebGis Intelligence, offering the ability not only to display the results but also to explain possible relationships, causes, and consequences of these results in a high-level, human-accessible language. It is possible to implement other technologies in the development of similar workflows, but in the selection of these, it is recommended that elements such as their maturity, robustness, flexibility, and documentation be considered.

5. Conclusions

In this study, we propose a new geoviewer tool for managing mangrove forests in Cuba, named SIGMEN. The methodology of this tool is based on the combination of remote sensing and open-source technologies such as MapStore, GeoServer, GeoNetwork, Django, and GEE, which allow monitoring of the spatial and temporal dynamics of mangroves in the Gran Humedal del Norte de Ciego de Ávila (GHNCA), a central province of Cuba. The modeling study combining spectral bands and vegetation indices with a Random Forest algorithm technique proved to be effective in accurately classifying and mapping mangrove-covered areas, achieving an outstanding overall accuracy of 94.11%. The features of SIGMEN facilitate the spatial and temporal visualizations and analysis of data, allowing for the determination of possible impacts of anthropogenic and environmental factors such

as temperature, precipitation regimes, and sea level rise on mangrove health. The novelty of this work lies in the application of these techniques and the development of the first tool specifically designed for mangrove monitoring in Cuba. Finally, this tool also supports the management and conservation actions of mangrove forests. SIGMEN is currently an initial version that will be progressively improved with the implementation of new methodologies and expanded for its use in other regions of Cuba and the Caribbean region.

Author Contributions: Conceptualization, A.V.-J., R.G.-L. and R.G.-D.Z.; methodology, A.V.-J. and R.G.-L.; software, A.V.-J. and R.G.-L.; maps, A.V.-J. and R.G.-L.; investigation, A.V.-J., R.G.-D.Z., R.G.-L., R.S., M.S. and F.M.-P.; statistical analysis, A.V.-J., R.G.-D.Z. and R.G.-L.; writing, A.V.-J., R.G.-D.Z., R.G.-L., R.S., M.S. and F.M.-P.; supervision, A.V.-J., R.G.-D.Z., R.G.-L., R.S., M.S. and F.M.-P. All authors have read and agreed to the published version of the manuscript.

Funding: This work was supported by the territorial project "Gestión ambiental integradora con enfoque ecosistémico en el Gran Humedal del Norte de Ciego de Ávila para su adaptación al cambio climático" of the Cuban government (Code: PT121CA003-003).

Data Availability Statement: The raw data supporting the conclusions of this article will be made available by the authors upon request. Codes for programming the Mangrove viewer are freely available at https://github.com/ragolodc/mangrove-monitor (accessed on 10 August 2024).

Acknowledgments: We extend our deepest gratitude to the Spanish Agency for International Development Cooperation (AECID) and the faculty of the Master in Geoinformatics for the Management of Natural Resources of the University of León, Spain. Without them, this research would not have been possible. M.S. is thankful for the support from the Xunta de Galicia (Consellería de Cultura, Educación, Formación Profesional e Universidades) under the Postdoctoral grants No. ED481D−2024/017). R.S. acknowledges the grant RYC2021−034044-I funded by Ministerio de Ciencia, Innovación y Universidades, Spain (MICIU/AEI/10.13039/501100011033) and the European Union Next Generation EU/PRTR. M.S and R.S also acknowledge the support from the project Excelencia-ED431F-2024/03 funded by the Xunta de Galicia.

Conflicts of Interest: The authors declare no conflicts of interest.

References

1. Intergovernmental Panel On Climate Change (IPCC). *Climate Change 2022—Impacts, Adaptation and Vulnerability: Working Group II Contribution to the Sixth Assessment Report of the Intergovernmental Panel on Climate Change*, 1st ed.; Cambridge University Press: Cambridge, UK, 2023; ISBN 978-1-00-932584-4.
2. The Convention on Wetlands, La Convención Sobre Los Humedales. Available online: https://www.ramsar.org/es (accessed on 20 July 2024).
3. Paleo, U.F.; Castiñeiras, L. (Eds.) *Family Farms and the Conservation of Agrobiodiversity in Cuba: Food Security and Nature*; Routledge: London, UK, 2023; ISBN 978-1-315-18388-6.
4. Walcker, R.; Laplanche, C.; Herteman, M.; Lambs, L.; Fromard, F. Damages Caused by Hurricane Irma in the Human-Degraded Mangroves of Saint Martin (Caribbean). *Sci. Rep.* **2019**, *9*, 18971. [CrossRef] [PubMed]
5. Matos-Pupo, F.; Peros, M.C.; González-De Zayas, R.; Valero-Jorge, A.; Pérez-López, O.E.; Álvarez-Taboada, F.; Sorí, R. Coastal Flooding Associated with Hurricane Irma in Central Cuba (Ciego de Ávila Province). *Atmosphere* **2023**, *14*, 1445. [CrossRef]
6. Godoy, J.C. Distribución, Composición Florística y Análisis Estructural Del Manglar de Las Lisas. Bachelor's Thesis, Universidad de San Carlos de Guatemala, Guatemala City, Guatemala, 1980.
7. Jiménez, J.A.; Jimenez, J.A. The Structure and Function of Dry Weather Mangroves on the Pacific Coast of Central America, with Emphasis on Avicennia Bicolor Forests. *Estuaries* **1990**, *13*, 182. [CrossRef]
8. Menéndez Carrera, L.; Guzmán, J.M. Ecosistema de Manglar En El Archipiélago Cubano Estudios y Experiencias Enfocados a Su Gestión. *Retrieved Diciembre* **2002**, *12*, 2018.
9. Guzmán, J.M.; Roig, E.Y.; Borroto-páez, R.; González-ferrer, S.; Martínez-daranas, B. Ecosistema de Manglar en el Archipiélago Cubano Estudios y Experiencias Enfocados a su Gestión. *Flora Habana Acad.* **2006**, *12*, 177.
10. Zulfa, A.W.; Norizah, K. Remotely Sensed Imagery Data Application in Mangrove Forest: A Review. *Pertanika J. Sci. Technol.* **2018**, *26*, 899–922.
11. Sunkur, R.; Kantamaneni, K.; Bokhoree, C.; Rathnayake, U.; Fernando, M. Mangrove Mapping and Monitoring Using Remote Sensing Techniques towards Climate Change Resilience. *Sci. Rep.* **2024**, *14*, 6949. [CrossRef]
12. Chen, K.; Dong, Z.; Gong, J. Monitoring Dynamic Mangrove Landscape Patterns in China: Effects of Natural and Anthropogenic Forcings during 1985–2020. *Ecol. Inform.* **2024**, *81*, 102582. [CrossRef]

13. Marvin, D.C.; Asner, G.P.; Knapp, D.E.; Anderson, C.B.; Martin, R.E.; Sinca, F.; Tupayachi, R. Amazonian Landscapes and the Bias in Field Studies of Forest Structure and Biomass. *Proc. Natl. Acad. Sci. USA* **2014**, *111*, E5224–E5232. [CrossRef]
14. Heumann, B.W. Satellite Remote Sensing of Mangrove Forests: Recent Advances and Future Opportunities. *Prog. Phys. Geogr. Earth Environ.* **2011**, *35*, 87–108. [CrossRef]
15. Hauser, L.T.; Féret, J.-B.; Binh, N.A.; van Der Windt, N.; Sil, Â.F.; Timmermans, J.; Soudzilovskaia, N.A.; van Bodegom, P.M. Towards Scalable Estimation of Plant Functional Diversity from Sentinel-2: In-Situ Validation in a Heterogeneous (Semi-)Natural Landscape. *Remote Sens. Environ.* **2021**, *262*, 112505. [CrossRef]
16. Roman, J. The Ecology and Conservation of Cuba's Coastal and Marine Ecosystems. *Bull. Mar. Sci.* **2018**, *94*, 149–169. [CrossRef]
17. Galford, G.L.; Fernandez, M.; Roman, J.; Monasterolo, I.; Ahamed, S.; Fiske, G.; González-Díaz, P.; Kaufman, L. Cuban Land Use and Conservation, from Rainforests to Coral Reefs. *Bull. Mar. Sci.* **2018**, *94*, 171–191. [CrossRef]
18. Jayakumar, K.; Malarvannan, S. A WebGIS Based Decision Support System for Land Use and Land Cover Changes: A Case Study of Tiruvallur Block, Tamil Nadu. *Int. J. Earth Sci. Eng.* **2015**, *8*, 1892–1898.
19. Kuenzer, C.; Bluemel, A.; Gebhardt, S.; Quoc, T.V.; Dech, S. Remote Sensing of Mangrove Ecosystems: A Review. *Remote Sens.* **2011**, *3*, 878–928. [CrossRef]
20. Denis Ávila, D.; Curbelo, E.A.; Madrigal-Roca, L.J.; Pérez-Lanyau, R.D. Variación Espacio-Temporal de La Respuesta Espectral En Manglares de La Habana, Cuba, Evaluada Con Sensores Remotos. *Rev. Biol. Trop.* **2020**, *68*, 321–335. [CrossRef]
21. Sartor, S.M.; Rosa, M.R.; Pires, J.T.; Oller Nascimento, C.A. Web Atlas Como Herramienta Para La Gestión Integrada Costera: De Los Datos al Conocimiento Práctico. *Rev. Costas* **2021**, *6*, 427–454. [CrossRef]
22. Gajbe, A.; Shankar, A.; Rodriguez, S. Virtual Coast Guard: An Open and Crowdsourced GIS Portal for Stewardship of I Ndia's Coast. *Trans. GIS* **2014**, *18*, 544–554. [CrossRef]
23. Balilo Jr, B.B.; Vibar, J.C.; Balmadrid, D.; Dioneda Sr, R.R.; Maraña, H.L.; Sy, D.J. Implementation of FishCORAL-PRSA Web-Based Information System for Asid Gulf Project. *Bicol Univ. R J.* **2018**, *22*, 44–57. [CrossRef]
24. Salzmann, U.; Krause, G.; Koch, B.P.; Rojo, I.P. The Mangrove Information System MAIS: Managing and Integrating Interdisciplinary Research Data. In *Mangrove Dynamics and Management in North Brazil*; Saint-Paul, U., Schneider, H., Eds.; Ecological Studies; Springer: Berlin/Heidelberg, Germany, 2010; Volume 211, pp. 355–364, ISBN 978-3-642-13456-2.
25. Jayakumar, K. Managing Mangrove Forests Using Open Source-Based WebGIS. In *Coastal Management*; Elsevier: Amsterdam, The Netherlands, 2019; pp. 301–321, ISBN 978-0-12-810473-6.
26. Caiza-Morales, L.; Gómez, C.; Torres, R.; Nicolau, A.P.; Olano, J.M. MANGLEE: A Tool for Mapping and Monitoring MANgrove Ecosystem on Google Earth Engine—A Case Study in Ecuador. *J. Geovisualization Spat. Anal.* **2024**, *8*, 17. [CrossRef]
27. Vidal Olivera, V.M.; González-Abreu Fernández, R. Relación del régimen hídrico actual con algunos impactos ambientales en el gran humedal del norte de Ciego de Ávila. 2010. Available online: https://aquadocs.org/handle/1834/3566 (accessed on 20 August 2024).
28. Vidal Olivera, V.M.; González-Abreu Fernández, R. Aguas Superficiales y Subterráneas En El Gran Humedal Del Norte de Ciego de Ávila. *Ing. Hidráulica Ambient.* **2013**, *34*, 57–69.
29. Gómez-Martín, M.B.; Matos-Pupo, F.; Bada-Díaz, R.; Escalante-Pérez, D. Assessing Present and Future Climate Conditions for Beach Tourism in Jardines Del Rey (Cuba). *Atmosphere* **2020**, *11*, 1295. [CrossRef]
30. Wege, D.C.; Anadon-Irizarri, V. *Important Bird Areas in the Caribbean: Key Sites for Conservation*; BirdLife International Cambridge: Cambridge, UK, 2008.
31. Menéndez-Pérez, H.; Díaz-Martínez, R.; González-de Zayas, R.; González-Fernández, J.A. Caracterización Hidroquímica Del Gran Humedal Del Norte, Ciego de Ávila, Cuba/Hydrochemical Characterization of the Northern Great Wetland, Ciego de Ávila, Cuba. *Min. Geol.* **2011**, *27*, 15–41.
32. Ferrer-Sánchez, Y.; Plasencia Vazquez, A.H.; Abasolo-Pacheco, F.; Denis Ávila, D.; Ruiz Companioni, I. Pertinencia Del Uso de Las Características Espectrales Del Hábitat Como Predictor de La Estructura En Comunidades de Aves de Un Humedal de Cuba. *Huitzil* **2017**, *18*, 141–156. [CrossRef]
33. Faife-Cabrera, M.; Pérez-Obregón, A.; González-Leiva, L. Diversidad Florística de Cayo Paredón Grande, Ciego de Ávila, Cuba. *Acta Botánica Cuba.* **2020**, *219*, 67–68.
34. Vidal Olivera, V.M.; Abreu Fernández, R.G.; Jiménez Peña, Y.; Valdés González, L.A.; Castro Carrillo, M. Funciones y Usos de Los Recursos Hídricos En El Gran Humedal Del Norte de Ciego de Ávila. *Ing. Hidráulica Ambient.* **2015**, *36*, 84–93.
35. Aguilar, D.G.; Soto, J.P.; Manrique, O.B.; Pérez, H.E.; Silva, M.L. Caracterización Ingenieríl de Obras Hidráulicas En La Provincia Ciego de Ávila. *Univ. Cienc.* **2024**, *13*, 109–121.
36. Gascon, F.; Bouzinac, C.; Thépaut, O.; Jung, M.; Francesconi, B.; Louis, J.; Lonjou, V.; Lafrance, B.; Massera, S.; Gaudel-Vacaresse, A. Copernicus Sentinel-2A Calibration and Products Validation Status. *Remote Sens.* **2017**, *9*, 584. [CrossRef]
37. Boto, K.G.; Wellington, J.T. Phosphorus and Nitrogen Nutritional Status of a Northern Australian Mangrove Forest. *Mar. Ecol. Prog. Ser. Oldendorf* **1983**, *11*, 63–69. [CrossRef]
38. Lovelock, C.E.; Feller, I.C.; McKee, K.L.; Thompson, R.C. Variation in Mangrove Forest Structure and Sediment Characteristics in Bocas Del Toro, Panama. *Caribb. J. Sci.* **2005**, *41*, 456–464.
39. Pool, D.J.; Snedaker, S.C.; Lugo, A.E. Structure of Mangrove Forests in Florida, Puerto Rico, Mexico, and Costa Rica. *Biotropica* **1977**, *9*, 195–212. [CrossRef]

40. Gorelick, N.; Hancher, M.; Dixon, M.; Ilyushchenko, S.; Thau, D.; Moore, R. Google Earth Engine: Planetary-Scale Geospatial Analysis for Everyone. *Remote Sens. Environ.* **2017**, *202*, 18–27. [CrossRef]
41. Liu, L.; Xiao, X.; Qin, Y.; Wang, J.; Xu, X.; Hu, Y.; Qiao, Z. Mapping Cropping Intensity in China Using Time Series Landsat and Sentinel-2 Images and Google Earth Engine. *Remote Sens. Environ.* **2020**, *239*, 111624. [CrossRef]
42. Gilabert, M.A.; Gonzalez-Piqueras, J.; García-Haro, J. Acerca de Los Índices de Vegetación. *Rev. Teledetec. Rev. Asoc. Esp. Teledetec.* **1997**, *8*, 1–10.
43. Rouse Jr, J.W.; Haas, R.H.; Deering, D. *Monitoring the Vernal Advancement and Retrogradation (Green Wave Effect) of Natural Vegetation*; Texas A&M University: College Station, TX, USA, 1974.
44. Huete, A.; Didan, K.; Miura, T.; Rodriguez, E.P.; Gao, X.; Ferreira, L.G. Overview of the Radiometric and Biophysical Performance of the MODIS Vegetation Indices. *Remote Sens. Environ.* **2002**, *83*, 195–213. [CrossRef]
45. Gitelson, A.A.; Viña, A.; Verma, S.B.; Rundquist, D.C.; Arkebauer, T.J.; Keydan, G.; Leavitt, B.; Ciganda, V.; Burba, G.G.; Suyker, A.E. Relationship between Gross Primary Production and Chlorophyll Content in Crops: Implications for the Synoptic Monitoring of Vegetation Productivity. *J. Geophys. Res. Atmospheres* **2006**, *111*, 2005JD006017. [CrossRef]
46. Klemas, V.; Smart, R. The Influence of Soil Salinity, Growth Form, and Leaf Moisture on-the Spectral Radiance Of. *Photogramm. Eng. Remote Sens.* **1983**, *49*, 77–83.
47. Pipia, L.; Amin, E.; Belda, S.; Salinero-Delgado, M.; Verrelst, J. Green LAI Mapping and Cloud Gap-Filling Using Gaussian Process Regression in Google Earth Engine. *Remote Sens.* **2021**, *13*, 403. [CrossRef]
48. R: The R Project for Statistical Computing. Available online: https://www.r-project.org/ (accessed on 30 July 2023).
49. Royimani, L.; Mutanga, O.; Odindi, J.; Dube, T.; Matongera, T.N. Advancements in Satellite Remote Sensing for Mapping and Monitoring of Alien Invasive Plant Species (AIPs). *Phys. Chem. Earth Parts ABC* **2019**, *112*, 237–245. [CrossRef]
50. Valero-Jorge, A.; González-De Zayas, R.; Matos-Pupo, F.; Becerra-González, A.L.; Álvarez-Taboada, F. Mapping and Monitoring of the Invasive Species Dichrostachys Cinerea (Marabú) in Central Cuba Using Landsat Imagery and Machine Learning (1994–2022). *Remote Sens.* **2024**, *16*, 798. [CrossRef]
51. Dai, W.; Xue, G.-R.; Yang, Q.; Yu, Y. Transferring Naive Bayes Classifiers for Text Classification. In Proceedings of the AAAI, Vancouver, BC, Canada, 22–26 July 2007; Volume 7, pp. 540–545.
52. Chen, X.; Jeong, J.C. Enhanced Recursive Feature Elimination. In Proceedings of the Sixth International Conference on Machine learning and Applications (ICMLA 2007), Cincinnati, OH, USA, 13–15 December 2007; IEEE: Piscataway, NJ, USA, 2007; pp. 429–435.
53. Tucker, C.J. Red and Photographic Infrared Linear Combinations for Monitoring Vegetation. *Remote Sens. Environ.* **1979**, *8*, 127–150. [CrossRef]
54. Roujean, J.-L.; Breon, F.-M. Estimating PAR Absorbed by Vegetation from Bidirectional Reflectance Measurements. *Remote Sens. Environ.* **1995**, *51*, 375–384. [CrossRef]
55. Chen, J.M. Evaluation of Vegetation Indices and a Modified Simple Ratio for Boreal Applications. *Can. J. Remote Sens.* **1996**, *22*, 229–242. [CrossRef]
56. Gao, B.-C. NDWI—A Normalized Difference Water Index for Remote Sensing of Vegetation Liquid Water from Space. *Remote Sens. Environ.* **1996**, *58*, 257–266. [CrossRef]
57. Gómez-Sánchez, E.; De Las Heras, J.; Lucas-Borja, M.; Moya, D. Ajuste de Metodologías Para Evaluar Severidad de Quemado En Zonas Semiáridas (SE Peninsular): Incendio Donceles 2012. *Rev. Teledetec.* **2017**, *49*, 103–113. [CrossRef]
58. Pérez, S.A.; Vega, J.; Rodríguez, F.; Fernández, C.; Vega-Nieva, D.; Ruiz-González, A. Validación de Los Índices de Teledetección dNBR y RdNBR Para Determinar La Severidad Del Fuego En El Incendio Forestal de Oia-O Rosal (Pontevedra) En 2013. *Rev. Teledetec.* **2017**, *49*, 49–61.
59. Cohen, J. A Coefficient of Agreement for Nominal Scales. *Educ. Psychol. Meas.* **1960**, *20*, 37–46. [CrossRef]
60. Chicco, D.; Jurman, G. The Advantages of the Matthews Correlation Coefficient (MCC) over F1 Score and Accuracy in Binary Classification Evaluation. *BMC Genom.* **2020**, *21*, 6. [CrossRef]
61. Yacouby, R.; Axman, D. *Probabilistic Extension of Precision, Recall, and F1 Score for More Thorough Evaluation of Classification Models*; Association for Computational Linguistics: Stroudsburg, PA, USA, 2020; pp. 79–91.
62. Chuvieco Salinero, E. *Teledetección Ambiental: La Observación de La Tierra Desde El Espacio*; ARIEL: Mount Vernon, OH, USA, 2010; 608p, ISBN 978-84-344-3498-1.
63. Demšar, J. Statistical Comparisons of Classifiers over Multiple Data Sets. *J. Mach. Learn. Res.* **2006**, *7*, 1–30.
64. Foody, G.M. Classification Accuracy Comparison: Hypothesis Tests and the Use of Confidence Intervals in Evaluations of Difference, Equivalence and Non-Inferiority. *Remote Sens. Environ.* **2009**, *113*, 1658–1663. [CrossRef]
65. Tonbul, H.; Colkesen, I.; Kavzoglu, T. Classification of Poplar Trees with Object-Based Ensemble Learning Algorithms Using Sentinel-2A Imagery. *J. Geod. Sci.* **2020**, *10*, 14–22. [CrossRef]
66. Paz Pellat, F.; Romero Sánchez, M.E.; Palacios Vélez, E. Alcances y Limitaciones de Los Índices Espectrales de La Vegetación: Marco Teórico. *Terra Latinoam* **2014**, *32*, 177–194.
67. Li, Z.; Shen, H.; Weng, Q.; Zhang, Y.; Dou, P.; Zhang, L. Cloud and Cloud Shadow Detection for Optical Satellite Imagery: Features, Algorithms, Validation, and Prospects. *ISPRS J. Photogramm. Remote Sens.* **2022**, *188*, 89–108. [CrossRef]
68. Sentinel-2: Cloud Probability | Earth Engine Data Catalog. Available online: https://developers.google.com/earth-engine/datasets/catalog/COPERNICUS_S2_CLOUD_PROBABILITY (accessed on 30 June 2024).

69. Skakun, S.; Wevers, J.; Brockmann, C.; Doxani, G.; Aleksandrov, M.; Batič, M.; Frantz, D.; Gascon, F.; Gómez-Chova, L.; Hagolle, O.; et al. Cloud Mask Intercomparison eXercise (CMIX): An Evaluation of Cloud Masking Algorithms for Landsat 8 and Sentinel-2. *Remote Sens. Environ.* **2022**, *274*, 112990. [CrossRef]
70. Harmonized Sentinel-2 MSI: MultiSpectral Instrument, Level-2A | Earth Engine Data Catalog. Available online: https://developers.google.com/earth-engine/datasets/catalog/COPERNICUS_S2_SR_HARMONIZED (accessed on 30 June 2024).
71. S2 Processing. Available online: https://sentiwiki.copernicus.eu/web/s2-processing (accessed on 30 June 2024).
72. Calvo Rubio, R. Herramienta Para Análisis de Vulnerabilidades En Aplicaciones Web. 2020. Available online: http://hdl.handle.net/10651/61121 (accessed on 30 June 2024).
73. Vacacela, E.; Tenecota, J.; Torres, J.; Pacheco, J.K.C. Automatización de Procesos de Investigación, Vinculación, Prácticas/Pasantías Preprofesionales Para Universidades Ecuatorianas. *Alternativas* **2018**, *19*, 35–44. [CrossRef]
74. Chandra, G.; Ochieng, E.; Tieszen, L.L.; Zhu, Z.; Singh, A.; Loveland, T.; Masek, J.; Duke, N. Status and Distribution of Mangrove Forests of the World Using Earth Observation Satellite Data. *Glob. Ecol. Biogeogr.* **2010**, *20*, 154–159. [CrossRef]
75. Nagendra, H.; Nagendran, S.; Paul, S.; Pareeth, S. Graying, Greening and Fragmentation in the Rapidly Expanding Indian City of Bangalore. *Landsc. Urban Plan.* **2012**, *105*, 400–406. [CrossRef]
76. Hamilton, S.E.; Casey, D. Creation of a High Spatio-temporal Resolution Global Database of Continuous Mangrove Forest Cover for the 21st Century (CGMFC-21). *Glob. Ecol. Biogeogr.* **2016**, *25*, 729–738. [CrossRef]
77. Rafdinal, R.; Linda, R.; Raynaldo, A.; Subrata, E. Spatio-Temporal Mapping of Mangrove Forest from 1989–2021 Using Landsat Imagery in Sambas Regency, West Kalimantan Province. In *Proceedings of the AIP Conference Proceedings*; AIP Publishing: Melville, NY, USA, 2024; Volume 3132.
78. Boston, T.; Van Dijk, A.; Thackway, R. U-Net Convolutional Neural Network for Mapping Natural Vegetation and Forest Types from Landsat Imagery in Southeastern Australia. *J. Imaging* **2024**, *10*, 143. [CrossRef] [PubMed]
79. Luo, Q.; Li, Z.; Huang, Z.; Abulaiti, Y.; Yang, Q.; Yu, S. Retrieval of Mangrove Leaf Area Index and Its Response to Typhoon Based on WorldView-3 Image. *Remote Sens. Appl. Soc. Environ.* **2023**, *30*, 100931. [CrossRef]
80. Long, K.; Chen, Z.; Zhang, H.; Zhang, M. Spatiotemporal Disturbances and Attribution Analysis of Mangrove in Southern China from 1986 to 2020 Based on Time-Series Landsat Imagery. *Sci. Total Environ.* **2024**, *912*, 169157. [CrossRef] [PubMed]
81. Yu, J.; Nie, S.; Liu, W.; Zhu, X.; Sun, Z.; Li, J.; Wang, C.; Xi, X.; Fan, H. Mapping Global Mangrove Canopy Height by Integrating Ice, Cloud, and Land Elevation Satellite-2 Photon-Counting LiDAR Data with Multi-Source Images. *Sci. Total Environ.* **2024**, *939*, 173487. [CrossRef] [PubMed]
82. Pinkeaw, S.; Boonrat, P.; Koedsin, W.; Huete, A. Semi-Automated Mangrove Mapping at National-Scale Using Sentinel-2, Sentinel-1, and SRTM Data with Google Earth Engine: A Case Study in Thailand. *Egypt. J. Remote Sens. Space Sci.* **2024**, *27*, 555–564. [CrossRef]
83. Hong, Y.; Que, X.; Wang, Z.; Ma, X.; Wang, H.; Salati, S.; Liu, J. Mangrove Extraction from Super-Resolution Images Generated by Deep Learning Models. *Ecol. Indic.* **2024**, *159*, 111714. [CrossRef]
84. Upadhyay, A.; Singh, S.; Singh, N.; Pal, A.K. Comparative Study of SVM and Naïve Bayes for Mangrove Detection Using Satellite Image. In *Advances in Information Communication Technology and Computing*; Goar, V., Kuri, M., Kumar, R., Senjyu, T., Eds.; Lecture Notes in Networks and Systems; Springer: Singapore, 2021; Volume 135, pp. 227–235. ISBN 9789811554209.
85. Memon, N.; Patel, S.B.; Patel, D.P. A Novel Approach of Polsar Image Classification Using Naïve Bayes Classifier. In *Mathematical Modeling, Computational Intelligence Techniques and Renewable Energy*; Sahni, M., Merigó, J.M., Jha, B.K., Verma, R., Eds.; Advances in Intelligent Systems and Computing; Springer: Singapore, 2021; Volume 1287, pp. 93–104. ISBN 9789811599521.
86. Liu, X.; Fatoyinbo, T.E.; Thomas, N.M.; Guan, W.W.; Zhan, Y.; Mondal, P.; Lagomasino, D.; Simard, M.; Trettin, C.C.; Deo, R. Large-Scale High-Resolution Coastal Mangrove Forests Mapping across West Africa with Machine Learning Ensemble and Satellite Big Data. *Front. Earth Sci.* **2021**, *8*, 560933. [CrossRef]
87. Utomo, D.P.; Handayani, T.; Susiloningtyas, D.; Mansessa, M.D.M. The Spatial Dynamics of Mangrove Forest in the Alas Purwo Banyuwangi National Park Marine Tourism Area Using Remote Sensing Images. In *Proceedings of the IOP Conference Series: Earth and Environmental Science*; IOP Publishing: Bristol, UK, 2021; Volume 771, p. 012012.
88. Elmahdy, S.I.; Ali, T.A.; Mohamed, M.M.; Howari, F.M.; Abouleish, M.; Simonet, D. Spatiotemporal Mapping and Monitoring of Mangrove Forests Changes from 1990 to 2019 in the Northern Emirates, UAE Using Random Forest, Kernel Logistic Regression and Naive Bayes Tree Models. *Front. Environ. Sci.* **2020**, *8*, 102. [CrossRef]
89. Torio, D.D. Modelling Canopy Density Variations from Remotely Sensed Data: Implications on Monitoring Floristic and Macro-Benthic Properties of Mangrove Ecosystems. Master's Thesis, International Institute for Geo-Information Science and Earth Observation (ITC), Enschede, Netherlands, 2007.
90. Barati, S.; Rayegani, B.; Saati, M.; Sharifi, A.; Nasri, M. Comparison the Accuracies of Different Spectral Indices for Estimation of Vegetation Cover Fraction in Sparse Vegetated Areas. *Egypt. J. Remote Sens. Space Sci.* **2011**, *14*, 49–56. [CrossRef]
91. Duro, D.C.; Coops, N.C.; Wulder, M.A.; Han, T. Development of a Large Area Biodiversity Monitoring System Driven by Remote Sensing. *Prog. Phys. Geogr. Earth Environ.* **2007**, *31*, 235–260. [CrossRef]
92. Gillespie, T.W.; Ostermann-Kelm, S.; Dong, C.; Willis, K.S.; Okin, G.S.; MacDonald, G.M. Monitoring Changes of NDVI in Protected Areas of Southern California. *Ecol. Indic.* **2018**, *88*, 485–494. [CrossRef]
93. Flores, D.D.C.; Benítez, E.A.C.; Sánchez, Y.F.; Ávila, D.D. Variaciones Espaciales y Temporales En El Índice de Vegetación de Diferencia Normalizada En Cuba. *Ecosistemas* **2020**, *29*, 1885.

94. Pasaribu, R.A.; Cakasana, N.; Maduppa, H.; Subhan, B.; Arafat, D.; Sangadji, M.S.; Savana, M.S. Mangrove Density Level and Area Change Analysis in Small Islands Case Study: Untung Jawa Island, Seribu Islands, DKI Jakarta. In *Proceedings of the IOP Conference Series: Earth and Environmental Science*; IOP Publishing: Bristol, UK, 2020; Volume 429, p. 012060.
95. Rahman, A.F.; Dragoni, D.; Didan, K.; Barreto-Munoz, A.; Hutabarat, J.A. Detecting Large Scale Conversion of Mangroves to Aquaculture with Change Point and Mixed-Pixel Analyses of High-Fidelity MODIS Data. *Remote Sens. Environ.* **2013**, *130*, 96–107. [CrossRef]
96. Pastor-Guzman, J.; Dash, J.; Atkinson, P.M. Remote Sensing of Mangrove Forest Phenology and Its Environmental Drivers. *Remote Sens. Environ.* **2018**, *205*, 71–84. [CrossRef]
97. Zhang, K.; Thapa, B.; Ross, M.; Gann, D. Remote Sensing of Seasonal Changes and Disturbances in Mangrove Forest: A Case Study from South Florida. *Ecosphere* **2016**, *7*, e01366. [CrossRef]
98. Aljahdali, M.O.; Munawar, S.; Khan, W.R. Monitoring Mangrove Forest Degradation and Regeneration: Landsat Time Series Analysis of Moisture and Vegetation Indices at Rabigh Lagoon, Red Sea. *Forests* **2021**, *12*, 52. [CrossRef]
99. Ali, A.; Nayyar, Z.A. Extraction of Mangrove Forest through Landsat 8 Mangrove Index (L8MI). *Arab. J. Geosci.* **2020**, *13*, 1132. [CrossRef]
100. Zhang, X.; Treitz, P.M.; Chen, D.; Quan, C.; Shi, L.; Li, X. Mapping Mangrove Forests Using Multi-Tidal Remotely-Sensed Data and a Decision-Tree-Based Procedure. *Int. J. Appl. Earth Obs. Geoinf.* **2017**, *62*, 201–214. [CrossRef]
101. Shi, T.; Liu, J.; Hu, Z.; Liu, H.; Wang, J.; Wu, G. New Spectral Metrics for Mangrove Forest Identification. *Remote Sens. Lett.* **2016**, *7*, 885–894. [CrossRef]
102. Vilfan, N.; Van der Tol, C.; Yang, P.; Wyber, R.; Malenovský, Z.; Robinson, S.A.; Verhoef, W. Extending Fluspect to Simulate Xanthophyll Driven Leaf Reflectance Dynamics. *Remote Sens. Environ.* **2018**, *211*, 345–356. [CrossRef]
103. Batllori-Sampedro, E.; Febles-Patrón, J.L. Límites Máximos Permisibles Para El Aprovechamiento Del Ecosistema de Manglar. *Gac. Ecol.* **2007**, *82*, 5–23.
104. Abd-El Monsef, H.; Smith, S.E. A New Approach for Estimating Mangrove Canopy Cover Using Landsat 8 Imagery. *Comput. Electron. Agric.* **2017**, *135*, 183–194. [CrossRef]
105. Arfan, A.; Toriman, M.E.; Maru, R.; Sukri Nyompa, U. Reflectance Characteristic of Mangrove Species Using Spectroradiometer HR-1024 in Suppa Coast, Pinrang, South Sulawesi, Indonesia. *Asian J. Appl. Sci.* **2015**, *3*, 642–648.
106. Tucker, C.J.; Townshend, J.R.G. Strategies for Monitoring Tropical Deforestation Using Satellite Data. *Int. J. Remote Sens.* **2000**, *21*, 1461–1471. [CrossRef]
107. Bayo, B.; Habib, W.; Mahmood, S. Spatio-Temporal Assessment of Mangrove Cover in the Gambia Using Combined Mangrove Recognition Index. *Adv. Remote Sens.* **2022**, *2*, 74–84.
108. Xing, H.; Hou, D.; Wang, S.; Yu, M.; Meng, F. O-LCMapping: A Google Earth Engine-Based Web Toolkit for Supporting Online Land Cover Classification. *Earth Sci. Inform.* **2021**, *14*, 529–541. [CrossRef]
109. Chen, B.; Xiao, X.; Li, X.; Pan, L.; Doughty, R.; Ma, J.; Dong, J.; Qin, Y.; Zhao, B.; Wu, Z.; et al. A Mangrove Forest Map of China in 2015: Analysis of Time Series Landsat 7/8 and Sentinel-1A Imagery in Google Earth Engine Cloud Computing Platform. *ISPRS J. Photogramm. Remote Sens.* **2017**, *131*, 104–120. [CrossRef]
110. Nababa, I.; Symeonakis, E.; Koukoulas, S.; Higginbottom, T.; Cavan, G.; Marsden, S. Land Cover Dynamics and Mangrove Degradation in the Niger Delta Region. *Remote Sens.* **2020**, *12*, 3619. [CrossRef]
111. Gawlikowski, J.; Ebel, P.; Schmitt, M.; Zhu, X.X. Explaining the Effects of Clouds on Remote Sensing Scene Classification. *IEEE J. Sel. Top. Appl. Earth Obs. Remote Sens.* **2022**, *15*, 9976–9986. [CrossRef]
112. Zhang, Y.; Song, Y.; Ye, C.; Liu, J. An Integrated Approach to Reconstructing Snow Cover under Clouds and Cloud Shadows on Sentinel-2 Time-Series Images in a Mountainous Area. *J. Hydrol.* **2023**, *619*, 129264. [CrossRef]
113. Zhang, Y.; Peñuelas, J. Combining Solar-Induced Chlorophyll Fluorescence and Optical Vegetation Indices to Better Understand Plant Phenological Responses to Global Change. *J. Remote Sens.* **2023**, *3*, 0085. [CrossRef]
114. Veenendaal, B.; Brovelli, M.A.; Li, S. Review of Web Mapping: Eras, Trends and Directions. *ISPRS Int. J. Geo-Inf.* **2017**, *6*, 317. [CrossRef]
115. Sukojo, B.M.; Lisakiyanto, D.R. Web-Based Geographic Information System Development of Hotspots Distribution for Monitoring Forest and Land Fires Using Leaflet JavaScript Library (Case Study: Ogan Komering Ilir Regency, South Sumatera). *IOP Conf. Ser. Earth Environ. Sci.* **2021**, *936*, 012010. [CrossRef]
116. Bayat, B.; Montzka, C.; Graf, A.; Giuliani, G.; Santoro, M.; Vereecken, H. One Decade (2011–2020) of European Agricultural Water Stress Monitoring by MSG-SEVIRI: Workflow Implementation on the Virtual Earth Laboratory (VLab) Platform. *Int. J. Digit. Earth* **2022**, *15*, 730–747. [CrossRef]
117. Mohanty, M.P.; Karmakar, S. WebFRIS: An Efficient Web-Based Decision Support Tool to Disseminate End-to-End Risk Information for Flood Management. *J. Environ. Manag.* **2021**, *288*, 112456. [CrossRef] [PubMed]
118. Giri, C. Recent Advancement in Mangrove Forests Mapping and Monitoring of the World Using Earth Observation Satellite Data. *Remote Sens.* **2021**, *13*, 563. [CrossRef]
119. Binh, T.T.; Truong, H.L.; Long, D.T. A WebGIS Solution for Estimation Landuse Affected by Salinity Intrusion: Case Study in Ben Tre Province, Vietnam. *J. Geogr. Inf. Syst.* **2020**, *12*, 188–201. [CrossRef]

120. Carrera, L.M.M. El Ecosistema de Manglar en el Archipiélago Cubano: Bases para su Gestión. Ph.D. Thesis, Universidad de Alicante, Alicante, Spain, 2013.
121. Environmental Defense Fund (EEF). *Sustainable Livelihoods in Cuba's Coastal Zones: The Challenge of Achieving Climate Resilience in Tourism, Energy, Fisheries, Agriculture, and Communities (Technical Report)*; Environmental Defense Fund: New York, NY, USA, 2023; p. 139.